Few-cycle optical rogue waves: Complex modified Korteweg–de Vries equation

Jingsong He,[1,*] Lihong Wang,[1] Linjing Li,[1] K. Porsezian,[2] and R. Erdélyi[3]
[1]*Department of Mathematics, Ningbo University, Ningbo, Zhejiang 315211, People's Republic of China*
[2]*Department of Physics, Pondicherry University, Pondicherry 605014, India*
[3]*Solar Physics and Space Plasma Research Centre, University of Sheffield, Sheffield S3 7RH, United Kingdom*
(Received 21 March 2014; published 18 June 2014)

In this paper, we consider the complex modified Korteweg–de Vries (mKdV) equation as a model of few-cycle optical pulses. Using the Lax pair, we construct a generalized Darboux transformation and systematically generate the first-, second-, and third-order rogue wave solutions and analyze the nature of evolution of higher-order rogue waves in detail. Based on detailed numerical and analytical investigations, we classify the higher-order rogue waves with respect to their intrinsic structure, namely, fundamental pattern, triangular pattern, and ring pattern. We also present several new patterns of the rogue wave according to the standard and nonstandard decomposition. The results of this paper explain the generalization of higher-order rogue waves in terms of rational solutions. We apply the contour line method to obtain the analytical formulas of the length and width of the first-order rogue wave of the complex mKdV and the nonlinear Schrödinger equations. In nonlinear optics, the higher-order rogue wave solutions found here will be very useful to generate high-power few-cycle optical pulses which will be applicable in the area of ultrashort pulse technology.

DOI: 10.1103/PhysRevE.89.062917 PACS number(s): 05.45.Yv, 42.65.Tg, 03.75.Lm, 87.14.gk

I. INTRODUCTION

The theory of nonlinear dynamics has attracted considerable interest and is fundamentally linked to several basic developments in the area of soliton theory. It is well known that the Korteweg–de Vries (KdV) equation, modified Korteweg–de Vries (mKdV) equation, sine Gordon equation, and the nonlinear Schrödinger (NLS) equation are the most typical and well-studied integrable evolution equations which describe nonlinear wave phenomena for a range of dispersive physical systems. Their stable multisoliton solutions play an important role in the study of nonlinear waves [1]. Further studies have also been carried out to examine the effects on these solitons due to dissipation, inhomogeneity, or nonuniformity present in nonlinear media [2,3].

The term "soliton" is a sophisticated mathematical concept that derives its name from the word "solitary wave," which is a localized wave of translation that arises from the balance between nonlinear and dispersive effects [1]. In spite of the initial theoretical investigations, the concept of solitary waves could not gain wide recognition for a number of years in the midst of excitement created by the development of electromagnetic concepts in those times. Korteweg and de Vries (1895) developed a mathematical model for the shallow water problem and demonstrated the possibility of solitary wave generation [4]. Next, the study of solitary waves really took off in the mid-1960s when Zabusky and Kruskal discovered the remarkably stable particlelike behavior of solitary waves [5]. They reported numerical experiments where solitary waves, described by the KdV equation, passed through each other unchanged in speed or shape, which led them to coin the word "soliton" to suggest such a unique property. In a follow-up study Zakharov and Shabat generalized the inverse scattering method in 1972 and also solved the NLS equation, demonstrating both its integrability and the existence of soliton solutions [6].

Following the above discoveries, solitary waves of all flavors advanced rapidly in many areas of science and technology. In nonlinear physics applications to many areas, e.g., hydrodynamics, biophysics, atomic physics, nonlinear optics, etc., have been developed. As of now, more than a few hundred nonlinear evolution equations (NEEs) have been shown to admit solitons and some of these theoretical equations are also responsible for the experimental discovery of solitons [1,7]. In general, nonlinear phenomena are often modeled by NEEs exhibiting a wide range of high complexities in terms of difference in linear and nonlinear effects. In the past four decades or so, the advent of high-speed computers, many advanced mathematical softwares, and a number of sophisticated and systematic analytical methods, which are well supported by experiments, have encouraged both theoreticians and experimentalists. Nonlinear science has experienced an explosive growth by the invention of several exciting and fascinating new concepts not just like solitons, but, e.g., dispersion-managed solitons, rogue waves, similaritons, supercontinuum generation, etc. [1]. Many of the completely integrable nonlinear partial differential equations (NPDEs) admit one of the most striking aspects of nonlinear phenomena, which describe solitons as universal characters and they are of great mathematical as well as physical interest. It is impossible to discuss all these manifestations exhaustively in this paper. We further restrict ourselves to the solitary wave manifestation in nonlinear optics. In the area of soliton research at the forefront right now is the study of optical solitons, where the highly sought-after goal is to use strong localized nonlinear optical pulses as the high-speed information-carrying bits in optical fibers.

Optical solitons are localized electromagnetic waves that propagate steadily in a nonlinear medium resulting from the robust balance between nonlinearity and linear broadening due to dispersion and diffraction. The existence of the optical soliton was first time found in 1973 when Hasegawa and Tappert demonstrated the propagation of a pulse through a

*Corresponding author: hejingsong@nbu.edu.cn

nonlinear optical fiber described by the NLS equation [8]. They performed a number of computer simulations demonstrating that nonlinear pulse transmission in optical fibers would be stable. Subsequently, after the fabrication of low-loss fiber, Mollenauer *et al.* in 1980 successfully confirmed this theoretical prediction of soliton propagation in a laboratory experiment [7]. Since then, fiber solitons have emerged as a very promising potential candidate in long-haul fiber optic communication systems.

Further, in addition to several important developments in soliton theory, the concept of modulational instability (MI) has also been widely used in many nonlinear systems to explain why experiments involving white coherent light supercontinuum generation (SCG) admit a triangular spectrum which can be described by the analytical expressions for the spectra of Akhmediev breather solutions at the point of extreme compression [1]. In the case of the NLS equation, Peregrine already in [9] had identified the role of MI in the formation of patterns resembling high-amplitude freak waves or rogue waves (RWs). RWs have recently been also reported in different areas of science. In particular, in photonic crystal fiber RWs are well established in connection with SCG [10]. This actually has stimulated research for RWs in other physical systems and has paved the way for a number important applications, including the control of RWs by means of SCG [11,12], as well as studies in, e.g., superfluid helium [13], Bose-Einstein condensates [14], plasmas [15,16], microwaves [17], capillary phenomena [18], telecommunication data streams [19], inhomogeneous media [20], water experiments [21], and so on. Recently, Kibler *et al.* [22], using a suitable experiment with optical fibers, were able to generate femtosecond pulses with strong temporal and spatial localization and near-ideal temporal Peregrine soliton characteristics.

For the past couple of years, several NEEs were shown to exhibit the RW-type rational solutions [23–39]. From the above listed works, it is clear that one of the possible generating mechanisms [40] for the higher-order RW is the interaction of multiple breathers possessing identical and very particular frequency of the underlying equation. Though the theory of solitons and many mathematical methods have been well used in connection with soliton theory for the past four decades or so, to the best of our knowledge, the dynamics of multi-RW evolutions has not yet been systematically investigated in integrable nonlinear systems [41].

Very recently, considering the propagation of few-cycle optical pulses in cubic nonlinear media and by developing multiple scaling approach to the Maxwell-Bloch-Heisenberg equation up to the third order in terms of expansion parameter, the complex mKdV equation was derived [42,43]. Circularly polarized few-cycle optical solitons were found which are valid for long pulses. Thus, it is more than worthy to systematically investigate the existence of the few-cycle optical RWs for this model, and this is the main purpose of the present paper.

The organization of this paper is as follows. In Sec. II, based on the parameterized Darboux transformation (DT) of the mKdV equation, the general formation of the solution is given. In Sec. III, we construct the higher-order RWs from a periodic seed with constant amplitude and analyze their structures in detail by choosing suitable system parameters. We provide detailed discussion about the obtained results in Secs. IV and V.

II. THE DARBOUX TRANSFORMATION

For our analysis, we begin with coupled complex mKdV equations of the form of

$$q_t + q_{xxx} - 6qrq_x = 0, \tag{1}$$

$$r_t + r_{xxx} - 6rqr_x = 0. \tag{2}$$

Under a reduction condition $q = -r^*$, the above coupled equations reduce to the complex mKdV

$$q_t + q_{xxx} + 6|q|^2 q_x = 0. \tag{3}$$

The complex mKdV equation is one of the well-known and completely integrable equations in soliton theory, which possesses all the basic characters of integrable models. From a physical point of view, the above equation has been derived for, e.g., the dynamical evolution of nonlinear lattices, plasma physics, fluid dynamics, ultrashort pulses in nonlinear optics, nonlinear transmission lines, and so on [41]. The Lax pair corresponding to the coupled mKdV equations is given by [41], i.e.,

$$\psi_x = M\psi, \tag{4}$$

$$\psi_t = (V_3\lambda^3 + V_2\lambda^2 + V_1\lambda + V_0)\psi = N\psi, \tag{5}$$

with

$$\psi = \begin{pmatrix}\phi_1\\ \phi_2\end{pmatrix}, \quad M = \begin{pmatrix}-i\lambda & q\\ r & i\lambda\end{pmatrix}, \quad V_3 = \begin{pmatrix}-4i & 0\\ 0 & 4i\end{pmatrix},$$

$$V_2 = \begin{pmatrix}0 & 4q\\ 4\gamma & 0\end{pmatrix}, \quad V_1 = \begin{pmatrix}-2iqr & 2iq_x\\ -2ir_x & 2iqr\end{pmatrix},$$

$$V_0 = \begin{pmatrix}-qr_x + q_xr & -q_{xx} + 2q^2r\\ -r_{xx} + 2qr^2 & qr_x - q_xr\end{pmatrix}.$$

Here λ is an arbitrary complex spectral parameter or also called eigenvalue, and ψ is the eigenfunction corresponding to λ of the complex mKdV equation. From the compatibility condition $M_t - N_x + [M,N] = 0$, one can easily obtain the coupled equations (1) and (2). Furthermore, we set T to be a gauge transformation by

$$\psi^{[1]} = T\psi, \quad q \to q^{[1]}, \quad r \to r^{[1]}, \tag{6}$$

and

$$\psi_x^{[1]} = M^{[1]}\psi^{[1]}, \quad M^{[1]} = (T_x + TM)T^{-1}, \tag{7}$$

$$\psi_t^{[1]} = N^{[1]}\psi^{[1]}, \quad N^{[1]} = (T_t + TN)T^{-1}. \tag{8}$$

Here $M^{[1]} = M(q \to q^{[1]}, r \to r^{[1]})$, $N^{[1]} = N(q \to q^{[1]}, r \to r^{[1]})$. By cross-differentiating (7) and (8), we obtain

$$M_t^{[1]} - N_x^{[1]} + [M^{[1]}, N^{[1]}] = T(M_t - N_x + [M,N])T^{-1}. \tag{9}$$

This implies that, in order to prove that the mKdV equation is invariant under the gauge transformation (6), it is important to determine the T such that $M^{[1]}$ and $N^{[1]}$ have the same forms as M and N. Meanwhile, the seed solutions (q, r) in spectral

matrices M and N are mapped into the new solutions ($q^{[1]}$, $r^{[1]}$) in terms of transformed spectral matrices $M^{[1]}$ and $N^{[1]}$.

Recently, using the generalized DT, nth-order RW solutions for the complex mKdV equation have been proposed in, e.g., [38]. However, in our work, we shall systematically analyze the evolution of the different patterns of higher-order RWs by suitably choosing the parameters in the rational solutions. In addition, it is worth noting that the obtained results are in agreement with our recently published developments about the method of generating higher-order RWs [39,40].

A. Onefold Darboux transformation

From the knowledge of the known form of the DT for the NLS equation [44–49], we assume that a trial Darboux matrix T in Eq. (6) has the form

$$T = T(\lambda) = \begin{pmatrix} a_1 & b_1 \\ c_1 & d_1 \end{pmatrix} \lambda + \begin{pmatrix} a_0 & b_0 \\ c_0 & d_0 \end{pmatrix}, \tag{10}$$

where a_0, b_0, c_0, d_0, a_1, b_1, c_1, d_1 are functions of x and t. From

$$T_x + TM = M^{[1]}T, \tag{11}$$

by comparing the coefficients of λ^j, $j = 2,1,0$, it yields

$$\begin{aligned}
&\lambda^2 : b_1 = 0, \quad c_1 = 0, \\
&\lambda^1 : a_{1x} = 0, \quad -2ib_0 + q_1d_1 - qa_1 = 0, \\
&\quad d_{1x} = 0, \quad -rd_1 + r_1a_1 + 2ic_0 = 0, \\
&\lambda^0 : q_1c_0 - a_{0x} - rb_0 = 0, \quad -b_{0x} + q_1d_0 - qa_0 = 0, \\
&\quad r_1a_0 - c_{0x} - rd_0 = 0, \quad r_1b_0 - d_{0x} - qc_0 = 0.
\end{aligned} \tag{12}$$

From the coefficients of λ^1, we conclude that a_1 and d_1 are functions of t only. Similarly, from

$$T_t + TN = N^{[1]}T, \tag{13}$$

and by comparing the coefficients of λ^j, $j = 3,2,1,0$, we obtain the following set of equations

$$\begin{aligned}
&\lambda^3 : q_1d_1 - qa_1 - 2ib_0 = 0, \quad r_1a_1 - rd_1 + 2ic_0 = 0, \\
&\lambda^2 : -q_1r_1a_1i + 2q_1c_0 + a_1qri - 2rb_0 = 0, \quad -a_1q_xi + 2q_1d_0 - 2qa_0 + q_{1x}d_1i = 0, \\
&\quad 2r_1a_0 - r_{1x}a_1i - 2rd_0 + d_1r_xi = 0, \quad q_1r_1d_1i + 2r_1b_0 - 2qc_0 - d_1qri = 0, \\
&\lambda^1 : -a_{1t} + r_1q_{1x}a_1 + a_1qr_x - a_1rq_x + 2iq_{1x}c + 2ib_0r_x - 2iq_1r_1a_0 + 2ia_0qr - q_1r_{1x}a_1 = 0, \\
&\quad -2iq_1r_1b_0 - 2ib_0qr + a_1q_{xx} + 2iq_{1x}d_0 - 2ia_0q_x - 2a_1q^2r - q_{1xx}d_1 + 2q_1^2r_1d_1 = 0, \\
&\quad -r_{1xx}a_1 + 2iq_1r_1c_0 + 2q_1r_1^2a_1 + 2iqrc_0 - 2ia_0r_{1x} + 2id_0r_x - 2d_1qr^2 + d_1r_{xx} = 0, \\
&\quad -d_{1t} - 2ic_0q_x + 2iq_1r_1d_0 - r_1q_{1x}d_1 - 2ir_{1x}b_0 - d_1qr_x + d_1rq_x - 2id_0qr + q_1r_{1x}d_1 = 0, \\
&\lambda^0 : -q_{1xx}c_0 + b_0r_{xx} + 2q_1^2r_1c_0 + a_0qr_x - 2b_0qr^2 + r_1q_{1x}a_0 - q_1r_{1x}a_0 - a_0rq_x - a_{0t} = 0, \\
&\quad a_0q_{xx} - b_0qr_x - b_0q_1r_{1x} - 2a_0q^2r + r_1q_{1x}b_0 + 2q_1^2r_1d_0 + b_0rq_x - q_{1xx}d_0 - b_{0t} = 0, \\
&\quad -r_{1xx}a_0 + d_0r_{xx} - r_1q_{1x}c_0 + 2q_1r_1^2a_0 + q_1r_{1x}c_0 - c_0rq_x + c_0qr_x - 2d_0qr^2 - c_{0t} = 0, \\
&\quad -r_1q_{1x}d_0 + q_1r_{1x}d_0 - r_{1xx}b_0 + 2q_1r_1^2b_0 + c_0q_{xx} + d_0rq_x - d_0qr_x - 2c_0q^2r - d_{0t} = 0.
\end{aligned} \tag{14}$$

By making use of Eqs. (12) and (14), one may obtain $a_{1x} = 0$, $d_{1x} = 0$, $a_{1t} = 0$, $d_{1t} = 0$, which implies that a_1 and d_1 are two constants.

In order to obtain the nontrivial solutions of the complex mKdV equation, we provide the DT under the condition $a_1 = 1$, $d_1 = 1$. Without loss of generality, and based on Eqs. (12) and (14), we observe that the Darboux matrix T admits the following form:

$$T = T(\lambda) = \begin{pmatrix} 1 & 0 \\ 0 & 1 \end{pmatrix} \lambda + \begin{pmatrix} a_0 & b_0 \\ c_0 & d_0 \end{pmatrix}. \tag{15}$$

Here a_0, b_0, c_0, d_0 are functions of x and t, which could be expressed by two eigenfunctions corresponding to λ_1 and λ_2. To begin with, we introduce $2n$ eigenfunctions ψ_j and $2n$ associated distinct eigenvalues λ_j as follows:

$$\begin{aligned}
&\psi_j = \begin{pmatrix} \phi_{j1} \\ \phi_{j2} \end{pmatrix}, \quad j = 1,2,\ldots,2n, \\
&\phi_{j1} = \phi_1(x,t,\lambda_j), \quad \phi_{j2} = \phi_2(x,t,\lambda_j).
\end{aligned} \tag{16}$$

Note $\phi_1(x,t,\lambda)$ and $\phi_2(x,t,\lambda)$ are two components of eigenfunction ψ associated with λ in Eqs. (4) and (5). Here it is worthwhile to note that since the eigenfunction

$$\psi_j = \begin{pmatrix} \phi_{j1} \\ \phi_{j2} \end{pmatrix}$$

is the solution of the eigenvalue equations (4) and (5) corresponding to λ_j, and the eigenfunction

$$\psi_j' = \begin{pmatrix} -\phi_{j2}^* \\ \phi_{j1}^* \end{pmatrix}$$

is also the solution of Eqs. (4) and (5) corresponding to λ_j^*, where $*$ denotes the complex conjugate.

We assume from now on that even number eigenfunctions and eigenvalues are given by odd ones as the following rule ($j = 1,2,\ldots,n$):

$$\begin{aligned}
&\lambda_{2j} = \lambda_{2j-1}^*, \quad \phi_{2j,1} = -\phi_{2j-1,2}^*(\lambda_{2j-1}), \\
&\phi_{2j,2} = \phi_{2j-1,1}^*(\lambda_{2j-1}).
\end{aligned} \tag{17}$$

For convenience and simplicity of our mathematical manipulations, we propose the following theorems.

Theorem 1. The elements of a onefold Darboux matrix are presented with the eigenfunction ψ_1 corresponding to the eigenvalue λ_1 as

$$a_0 = -\frac{1}{\Delta_2}\begin{vmatrix}\lambda_1\phi_{11} & \phi_{12}\\ \lambda_2\phi_{21} & \phi_{22}\end{vmatrix}, \quad b_0 = \frac{1}{\Delta_2}\begin{vmatrix}\lambda_1\phi_{11} & \phi_{11}\\ \lambda_2\phi_{21x} & \phi_{21}\end{vmatrix},$$
$$c_0 = \frac{1}{\Delta_2}\begin{vmatrix}\phi_{12} & \lambda_1\phi_{12}\\ \phi_{22} & \lambda_2\phi_{22}\end{vmatrix}, \quad d_0 = -\frac{1}{\Delta_2}\begin{vmatrix}\phi_{11} & \lambda_1\phi_{12}\\ \phi_{21} & \lambda_2\phi_{22}\end{vmatrix}, \tag{18}$$

$$\Leftrightarrow T_1(\lambda;\lambda_1) = \begin{pmatrix}\lambda - \frac{1}{\Delta_2}\begin{vmatrix}\lambda_1\phi_{11} & \phi_{12}\\ \lambda_2\phi_{21} & \phi_{22}\end{vmatrix} & \frac{1}{\Delta_2}\begin{vmatrix}\lambda_1\phi_{11} & \phi_{11}\\ \lambda_2\phi_{21} & \phi_{21}\end{vmatrix}\\ \frac{1}{\Delta_2}\begin{vmatrix}\phi_{12} & \lambda_1\phi_{12}\\ \phi_{22} & \lambda_2\phi_{22}\end{vmatrix} & \lambda - \frac{1}{\Delta_2}\begin{vmatrix}\phi_{11} & \lambda_1\phi_{12}\\ \phi_{21} & \lambda_2\phi_{22}\end{vmatrix}\end{pmatrix}, \tag{19}$$

with $\Delta_2 = \begin{vmatrix}\phi_{11} & \phi_{12}\\ \phi_{21} & \phi_{22}\end{vmatrix}$, and then the new solutions $q^{[1]}$ and $r^{[1]}$ are given by

$$q^{[1]} = q + 2i\frac{1}{\Delta_2}\begin{vmatrix}\lambda_1\phi_{11} & \phi_{11}\\ \lambda_2\phi_{21} & \phi_{21}\end{vmatrix},$$
$$r^{[1]} = r - 2i\frac{1}{\Delta_2}\begin{vmatrix}\phi_{12} & \lambda_1\phi_{12}\\ \phi_{22} & \lambda_2\phi_{22}\end{vmatrix}, \tag{20}$$

and the new eigenfunction $\psi_j^{[1]}$ corresponding to λ_j is

$$\psi_j^{[1]} = T_1(\lambda;\lambda_1)|_{\lambda=\lambda_j}\psi_j. \tag{21}$$

Proof. Note that $b_1 = c_1 = 0$, $a_{1x} = 0$, and $d_{1x} = 0$ are derived from the functional form of x, then $a_{1t} = 0$ and $d_{1t} = 0$ are derived from the functional form of t. So, a_1 and d_1 are arbitrary constants, and hence we let $a_1 = d_1 = 1$ for simplicity for later calculations. By transformation defined by Eqs. (12) and (14), new solutions are given by

$$q_1 = q + 2ib_0, \quad r_1 = r - 2ic_0. \tag{22}$$

By making use of the general property of the DT, i.e., $T_1(\lambda;\lambda_j)|_{\lambda=\lambda_1}\psi_j = 0, j = 1,2$, after some manipulations, Eq. (18) is obtained. Next, substituting (a_0,b_0,c_0,d_0) given in Eq. (18) into Eq. (22), the new solutions are given as in Eq. (20). Furthermore, by using the explicit matrix representation Eq. (19) of T_1, then $\psi_j^{[1]}(j \geqslant 3)$ is given by $\psi_j^{[1]} = T_1(\lambda;\lambda_1)|_{\lambda=\lambda_j}\psi_j$. ■

It is trivial to confirm $q^{[1]} = -(r^{[1]})^*$ by using the special choice on ψ_2 and λ_2 in Eq. (17). This means $q^{[1]}$ generates a new solution of the complex mKdV from a seed solution q. Note that $\psi_j^{[1]} = 0$ for $j = 1,2$.

B. *n*-fold Darboux transformation

By n-times iteration of the onefold DT T_1, we obtain n-fold DT T_n of the complex mKdV equation with the special choice on λ_{2j} and ψ_{2j} in Eq. (17). To save space, we omit the tedious calculation of T_n and its determinant representation. Under the above conditions, the reduction condition $q^{[n]} = -(r^{[n]})^*$ is preserved by T_n, so we just give $q^{[n]}$ in the following theorem.

Theorem 2. Under the choice of Eq. (17), the n-fold DT T_n generates a new solution of the complex mKdV equation from a seed solution q as

$$q^{[n]} = q - 2i\frac{N_{2n}}{D_{2n}}, \tag{23}$$

where

$$N_{2n} = \begin{vmatrix}\phi_{11} & \phi_{12} & \lambda_1\phi_{11} & \lambda_1\phi_{12} & \dots & \lambda_1^{n-1}\phi_{11} & \lambda_1^n\phi_{11}\\ \phi_{21} & \phi_{22} & \lambda_2\phi_{21} & \lambda_2\phi_{22} & \dots & \lambda_2^{n-1}\phi_{21} & \lambda_2^n\phi_{21}\\ \phi_{31} & \phi_{32} & \lambda_3\phi_{31} & \lambda_3\phi_{32} & \dots & \lambda_3^{n-1}\phi_{31} & \lambda_3^n\phi_{31}\\ \phi_{41} & \phi_{42} & \lambda_4\phi_{41} & \lambda_4\phi_{42} & \dots & \lambda_4^{n-1}\phi_{41} & \lambda_4^n\phi_{41}\\ \vdots & \vdots & \vdots & \vdots & \vdots & \vdots & \vdots\\ \phi_{2n1} & \phi_{2n2} & \lambda_{2n}\phi_{2n1} & \lambda_{2n}\phi_{2n2} & \dots & \lambda_{2n}^{n-1}\phi_{2n1} & \lambda_{2n}^n\phi_{2n1}\end{vmatrix},$$

$$D_{2n} = \begin{vmatrix}\phi_{11} & \phi_{12} & \lambda_1\phi_{11} & \lambda_1\phi_{12} & \dots & \lambda_1^{n-1}\phi_{11} & \lambda_1^{n-1}\phi_{12}\\ \phi_{21} & \phi_{22} & \lambda_2\phi_{21} & \lambda_2\phi_{22} & \dots & \lambda_2^{n-1}\phi_{21} & \lambda_2^{n-1}\phi_{22}\\ \phi_{31} & \phi_{32} & \lambda_3\phi_{31} & \lambda_3\phi_{32} & \dots & \lambda_3^{n-1}\phi_{31} & \lambda_3^{n-1}\phi_{32}\\ \phi_{41} & \phi_{42} & \lambda_4\phi_{41} & \lambda_4\phi_{42} & \dots & \lambda_4^{n-1}\phi_{41} & \lambda_4^{n-1}\phi_{42}\\ \vdots & \vdots & \vdots & \vdots & \vdots & \vdots & \vdots\\ \phi_{2n1} & \phi_{2n2} & \lambda_{2n}\phi_{2n1} & \lambda_{2n}\phi_{2n2} & \dots & \lambda_{2n}^{n-1}\phi_{2n1} & \lambda_{2n}^{n-1}\phi_{2n2}\end{vmatrix}.$$

By making use of Theorem 2 with a suitable seed solution, we can generate the multisolitons, multibreathers, and multi-RWs of the complex mKdV equation. As the multisoliton and multibreather solutions are well known and completely explored for the complex mKdV equation, next we concentrate mainly on the systematic construction of the higher-order RWs from the double degeneration [40] of the DT. Though the construction of higher-order RW solutions is quite cumbersome, one can still validate the correctness of these solutions with the help of modern computer tools such as a simple symbolic calculation or equivalent, and also by a direct numerical computation.

III. HIGHER-ORDER ROGUE WAVES

In this section, starting with a nonzero seed $q = ce^{i\rho}$, $\rho = ax + bt$, $b = a^3 - 6ac^2$, $a,b,c \in \mathbb{R}$, we shall present higher-order RWs of the complex mKdV equation. If $a = 0$, $q = c$ is a constant, which is just a seed solution to generate soliton. So, in this paper, we choose $a \neq 0$. By using the principle of superposition of the linear differential equations, the new eigenfunctions corresponding to λ_j can be provided by

$$\psi_j = \begin{pmatrix} d_1 c e^{i[(\frac{1}{2}a+c_1)x+(\frac{1}{2}b+2c_1c_2)t]} + d_2 i(\frac{1}{2}a+\lambda_j+c_1)e^{i[(-\frac{1}{2}a+c_1)x+(-\frac{1}{2}b+2c_1c_2)t]} \\ d_1 i(\frac{1}{2}a+\lambda_j+c_1)e^{-i[(-\frac{1}{2}a+c_1)x+(-\frac{1}{2}b+2c_1c_2)t]} + d_2 c e^{-i[(\frac{1}{2}a+c_1)x+(\frac{1}{2}b+2c_1c_2)t]} \end{pmatrix}, \tag{24}$$

with

$$\begin{aligned} d_1 &= e^{ic_1(s_0+s_1\varepsilon+s_2\varepsilon^2+\cdots+s_{n-1}\varepsilon^{n-1})}, \\ d_2 &= e^{-ic_1(s_0+s_1\varepsilon+s_2\varepsilon^2+\cdots+s_{n-1}\varepsilon^{n-1})}, \\ c_1 &= \frac{1}{2}\sqrt{a^2+4c^2+4\lambda_j a+4\lambda_j^2}, \\ c_2 &= 2\lambda_j^2 - c^2 + \frac{1}{2}a^2 - \lambda_j a. \end{aligned} \tag{25}$$

Here $s_i \in \mathcal{C}(i = 0,1,2,\ldots,n-1)$,$a,b,c \in \mathbb{R}$ are the arbitrary constants, ε is an infinitesimal parameter.

We are now in a position to consider the double degeneration of $q^{[n]}$ to obtain higher-order RW as in our earlier investigations [40]. It is trivial to check that $\psi_j(\lambda_0) = 0$ in Eq. (24), which means that these eigenfunctions are degenerate at $\lambda_0 = ic - \frac{a}{2}$. Setting $\lambda_{2j-1} \to \lambda_0$ and substituting $\psi_{2j-1}(j = 1,2,\ldots,n)$ defined by Eq. (24) back into Eq. (23), the double degeneration, i.e., eigenvalue and eigenfunction degeneration, occurs in $q^{[n]}$. Next, $q^{[n]}$ now becomes an indeterminate form $\frac{0}{0}$. We set $\lambda_{2j-1} = \lambda_0 + \epsilon$ and set ψ_{2j-1} to be given by Eq. (24); we obtain nth-order RW solutions by higher-order Taylor expansion of $q^{[n]}$ with respect to ϵ.

Theorem 3. An n-fold degenerate DT with a given eigenvalue λ_0 is realized in the degenerate limit $\lambda_j \to \lambda_0$ of T_n. This degenerate n-fold DT yields a new solution $q^{[n]}$ of the mKdV equation starting with the seed solution q, where

$$q^{[n]}(x,t;\lambda_0) = q - 2i\frac{N'_{2n}}{D'_{2n}}, \tag{26}$$

with

$$\begin{aligned} D'_{2n} &= \left[\frac{\partial^{n_i}}{\partial\varepsilon^{n_i}}\bigg|_{\varepsilon=0}(D_{2n})_{ij}(\lambda_0+\epsilon)\right]_{2n\times 2n}, \\ N'_{2n} &= \left[\frac{\partial^{n_i}}{\partial\varepsilon^{n_i}}\bigg|_{\varepsilon=0}(N_{2n})_{ij}(\lambda_0+\epsilon)\right]_{2n\times 2n}. \end{aligned}$$

Here $n_i = [\frac{i+1}{2}]$, $[i]$ denotes the floor function of i.

In the following, to avoid the tedious mathematical steps we encountered, we only present the expressions of the first-, second-, and third-order RWs by using Theorem 3. In each case, the solution $q^{[n]}$ describes the envelope of the RW, and its square modulus contains information such as, e.g., wave evolution above water surface, or the intensity of few-cycle optical wave, etc.

First, we set $n = 1$, D_2, and N_2 to take the form of 2×2 determinants. By using the first-order Taylor expansion with respect to ϵ in terms of elements of D_2 and N_2 through $\lambda_1 = \lambda_0 + \epsilon$, we determined N'_2 and D'_2 by equating the coefficient of $\sqrt{\epsilon}$, and then obtained the explicit expression for the first-order RW as

$$q^{[1]} = -ce^{ia[x+t(a^2-6c^2)]}\frac{A+48ic^2ta-3}{A+1}, \tag{27}$$

with $A = 24ta^2c^2x + 24ta^2c^2s_0 + 36t^2a^4c^2 - 48c^4tx - 48c^4ts_0 + 8c^2xs_0 + 144c^6t^2 + 4c^2x^2 + 4c^2s_0^2$.

Its evolution is presented in Fig. 1 (left) with the condition $d_1 = d_2 = 1$ and the Taylor expansion at $\lambda_0 = ic - \frac{a}{2} + \varepsilon$, in order to compare this with higher-order RWs. It is trivial to find that $|q^{[1]}|^2 = c^2$ when $x \to \infty$ and $t \to \infty$. This means that the asymptotic plane of $|q^{[1]}|^2$ has the height c^2. Particularly, let $a = 0$ and $s_0 = 0$; $|q^{[1]}|^2$ is a soliton propagating along a line $x = 6c^2t$ with a nonvanishing boundary. We set $c = -1$,$a = \sqrt{6}$,$s_0 = 0$, and $t \to t/2$, then $q^{[1]}$ gives $u[2]$ of Ref. [38].

When $n = 2$, we construct the second-order RWs under the assumption $d_1 = e^{ic_1(s_0+s_1\varepsilon)}$, $d_2 = e^{-ic_1(s_0+s_1\varepsilon)}$,$s_0 = 0$ from Theorem 3. An explicit form of $q^{[2]}$ is constructed as

$$q^{[2]} = ce^{ia[x+t(a^2-6c^2)]}\frac{B}{C}. \tag{28}$$

Here B and C are two degree 6 polynomials in x and t, which are given in Appendix A. From Fig. 1 (right), one finds that under the assumption $d_1 = 1$,$d_2 = 1$, or equivalently $s_0 = s_1 = 0$, the second-order rational solution admits a single high maximum at the origin. By suitably adjusting the parameter a one could control the decaying rate of the profile in the (x,t) plane. This is a fundamental pattern. Furthermore, as is shown in Fig. 8, when taking $d_1 \neq 1$ and $d_2 \neq 1$, the large peak of the second RW is completely separated and forms a set of three first-order rational solutions for sufficiently large s_1; meanwhile, $s_0 = 0$ and actually forms an equilateral triangle.

When $n = 3$ and $d_1 = e^{ic_1(s_0+s_1\varepsilon+s_2\varepsilon^2)}$ and $d_2 = e^{-ic_1(s_0+s_1\varepsilon+s_2\varepsilon^2)}$, then Theorem 3 yields an explicit formula of the third-order RW with parameters a,c,s_0,s_1,s_2. When $a = 1.5$,$c = 1$,$s_0 = s_1 = s_2 = 0$, we have

$$q^{[3]} = \frac{L_1}{L_2}e^{i(\frac{3}{2}x-\frac{45}{8}t)}. \tag{29}$$

Here L_1 and L_2 are two degree 12 polynomials in x and t, which are given in Appendix B. This is the fundamental pattern of the third-order RW, which is plotted in Fig. 2 (left) with a different value of a.

In general, Theorem 3 provides an efficient tool to produce analytical forms of higher-order RWs of the complex mKdV equation. Actually, we have also constructed the analytical formulas for fourth-, fifth-, and sixth-order RWs. However, because of their long expressions describing these solutions, we do not present them here but would provide them upon

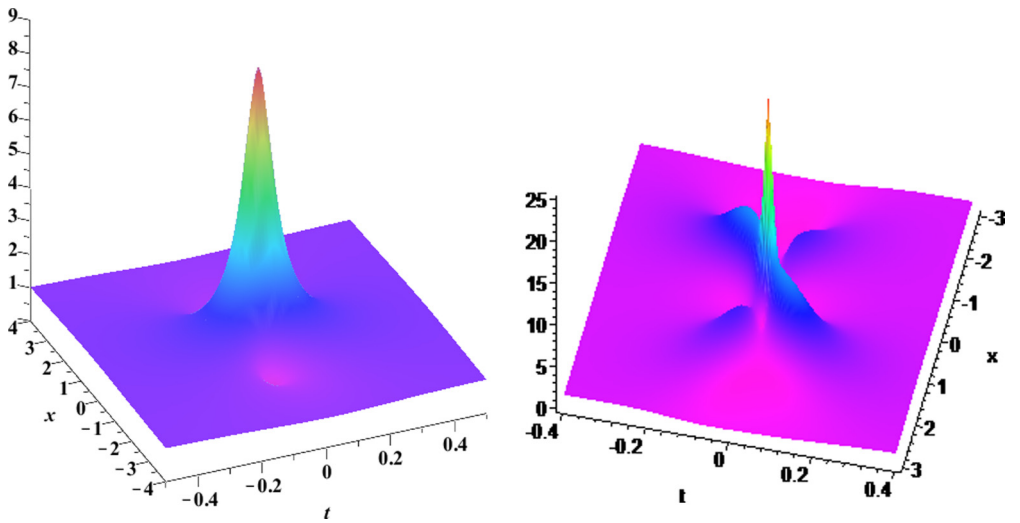

FIG. 1. (Color online) Fundamental pattern of the RW. The left panel is the evolution of $|q^{[1]}|^2$ (first-order RW), with specific parameters $a = 1.5, c = 1, s_0 = 0$. The right panel is $|q^{[2]}|^2$ (second-order RW), with specific parameters $a = 1.44, c = 1, s_0 = 0, s_1 = 0$.

request. The validity of all these higher-order RWs has been verified by symbolic computation. According to the explicit formulas of the nth-order RWs under fundamental patterns, we find that their maximum amplitude is $(2n+1)^2c^2 (n = 1,2,3,4,5,6)$ by setting $x = 0$ and $t = 0$ in $|q^{[n]}|^2$, and the height of the asymptotic plane is c^2, which is the same as that of the RW of the NLS equation. This fact can be easily verified through Figs. 1–3. All figures in this paper are plotted based on these explicit analytical formulas of the solutions. Once the explicit analytical higher-order RWs are known, our next aim is to generate and understand underlying the dynamics of the obtained different patterns by suitably selecting the value of s_i.

IV. RESULTS AND DISCUSSION

The above discussion is a clear manifestation of the evolution of the higher-order RWs from the Taylor expansion of the degenerate breather solutions. A brief discussion about the generating mechanism of higher-order RWs from the NEE has already been reported by [40]. For our purpose now, we customize our discussion only up to sixth-order RWs, since higher-order RWs are difficult to construct owing to the extreme complexity and tedious mathematical calculations. It is quite obvious from our numerical analysis that the choice of parameters such as d_1 and d_2 actually do generate three different basic patterns of RW solutions. Let us discuss these patterns now.

Fundamental patterns. When, e.g., $d_1 = d_2 = 1$, or equivalently $s_i = 0$ $(i = 0,1,2,\ldots,n-1)$ in $q^{[n]}$, the rational solutions of any order n have similar structures. In addition, there are $\frac{n(n+1)}{2} - 1$ local maxima on each side of the line at $t = 0$. Starting from ∞, before the central optimum high amplitude, there is a sequence of peaks with gradual increase in height. Here one can observe that the number of first peaks is n; then there is a row of $n-1$ symmetric peaks with respect to time t as shown in Figs. 1–3 for sixth-order RWs.

There are only two parameters a and c in the explicit forms of the RWs under fundamental patterns. It is a challenge problem to illustrate analytically the role of a and c in the control of the profile for the higher-order RWs due to the extreme complexity of the explicit forms of the nth-order RWs $(n \geqslant 2)$. So, we only study this problem for the first-order RW $|q^{[1]}|^2$. To this end, we introduce a method, i.e., the contour

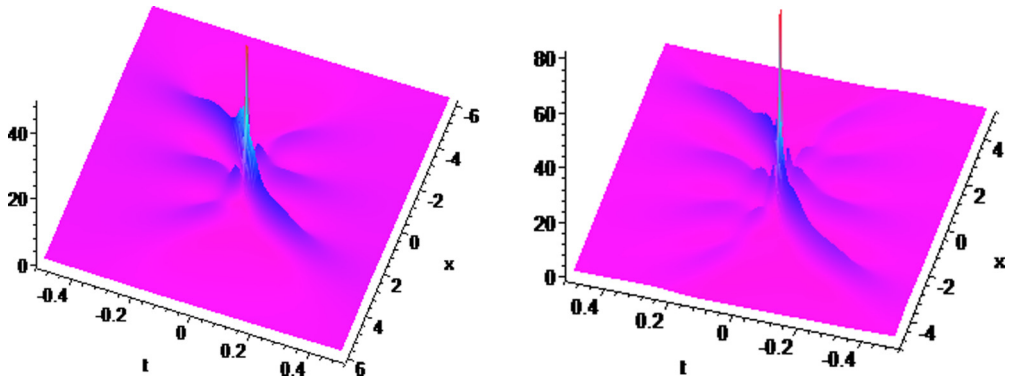

FIG. 2. (Color online) Fundamental pattern of the RW. The left panel is the evolution of $|q^{[3]}|^2$ (third-order RW), with specific parameters $a = 1.4, c = 1, s_0 = 0, s_1 = 0, s_2 = 0$. The right panel is $|q^{[4]}|^2$ (fourth-order RW), with specific parameters $a = 1.48, c = 1, s_0 = 0, s_1 = 0, s_2 = 0, s_3 = 0$.

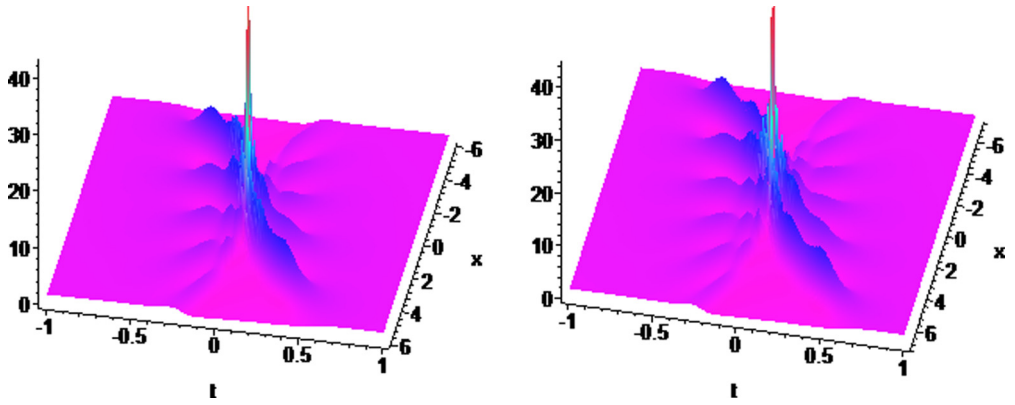

FIG. 3. (Color online) Fundamental patterns of the RWs. The left panel is the evolution of $|q^{[5]}|^2$ (fifth-order RW), with specific parameters $a = 1.5, c = 1, s_0 = 0, s_1 = 0, s_2 = 0, s_3 = 0, s_4 = 0$. The right panel is $|q^{[6]}|^2$ (sixth-order RW), with specific parameters $a = 1.5, c = 1, s_0 = 0, s_1 = 0, s_2 = 0, s_3 = 0, s_4 = 0, s_5 = 0$.

line method, to analyze the contour profile of the red bright spots in the density plot of Fig. 4, which intuitively shows the localization characters such as length and width of the RW. On the background plane with height c^2, a contour line of $|q^{[1]}|^2$ with $c = 1$ is a hyperbola,

$$x^2 - 12tx + 6ta^2x + 36t^2 - 72t^2a^2 + 9t^2a^4 - \tfrac{1}{4} = 0, \tag{30}$$

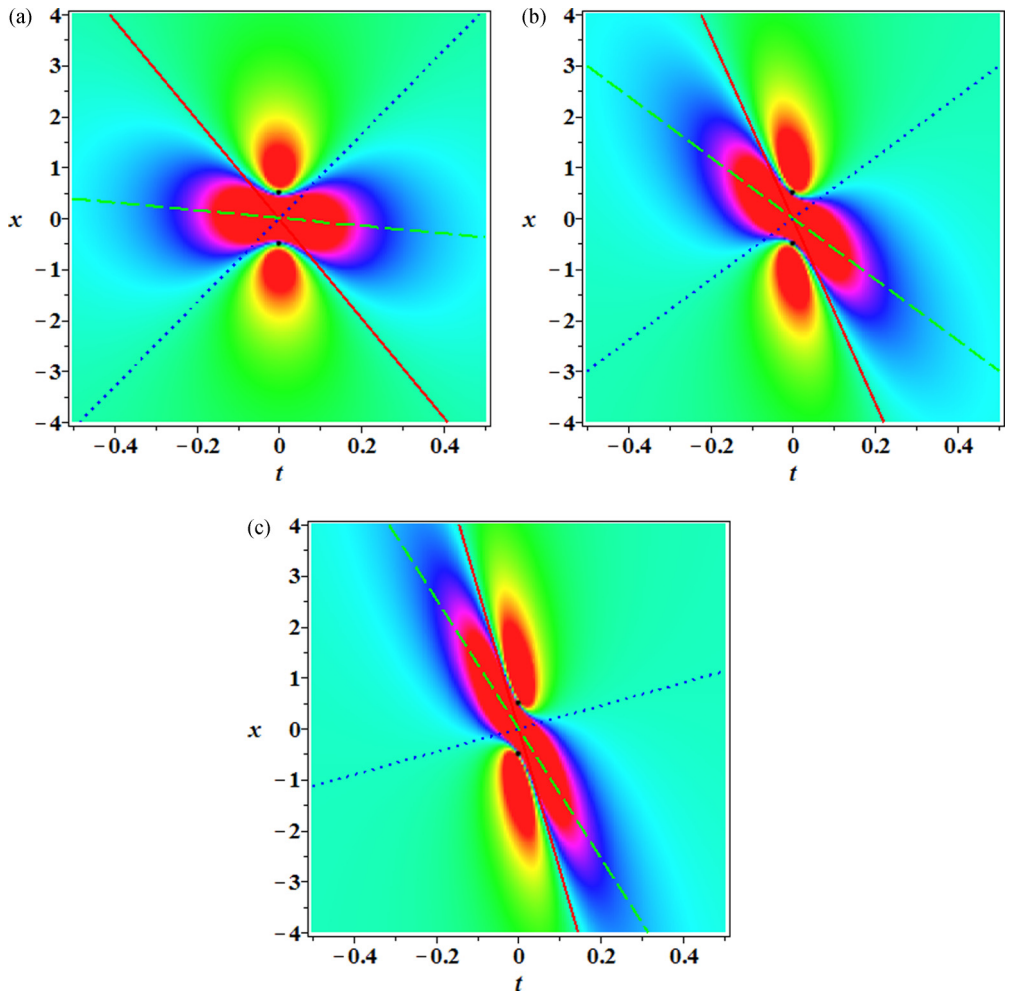

FIG. 4. (Color online) The density plots of the first-order RW $|q^{[1]}|^2$ with $c = 1$ and different values of a. From panels (a) to (c), $a = 1.5, 2, 2.5$ in order. Here red (solid) and blue (dotted) lines are plotted for two asymptotes of contour lines at height c^2, green (dashed) line are plotted for a median of one triangle composed of above two asymptotes and a parallel line of x axis except $t = 0$. Two fixed pints are located at $(0, 0.5)$ and $(0, -0.5)$ in the three panels.

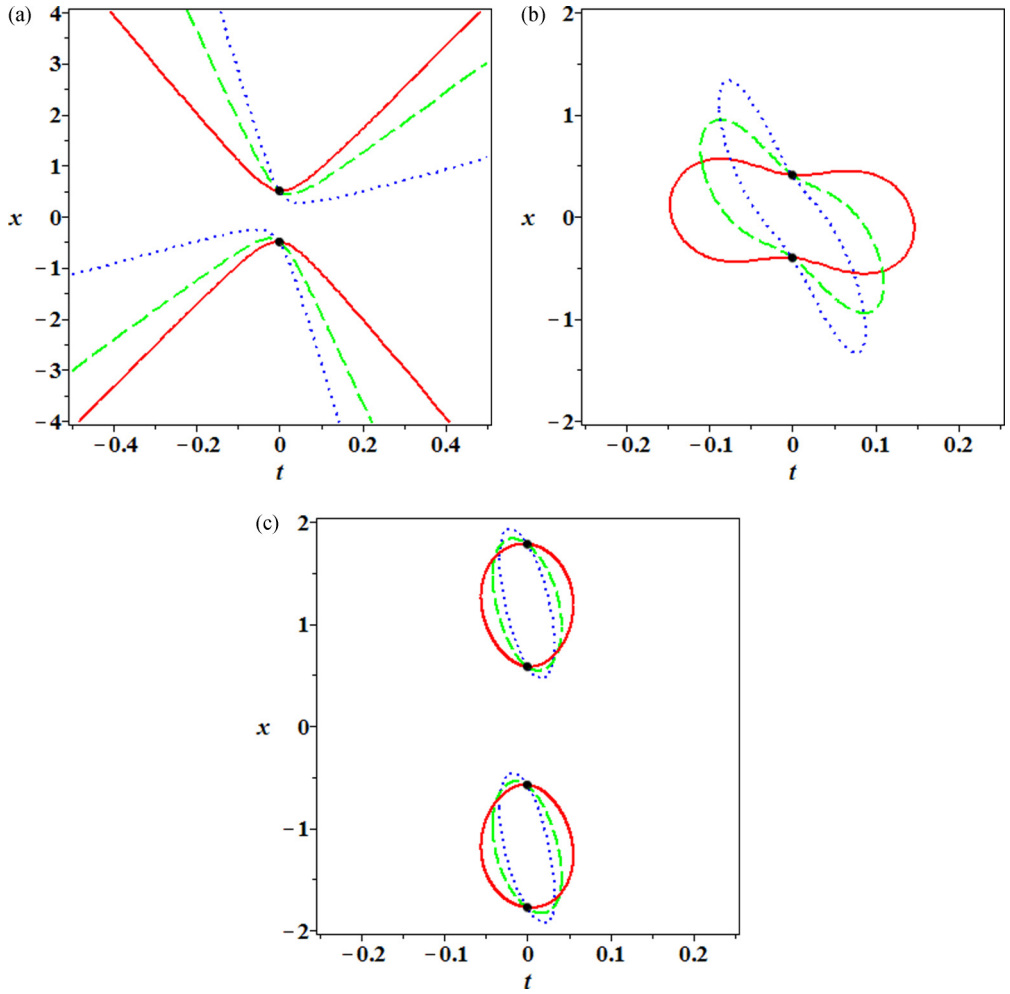

FIG. 5. (Color online) Contour lines of the first-order RW with $c = 1$ and $a = 1.5$ (red solid line), 2 (dash ed green line), 2.5 (dotted blue line). From panels (a) to (c), panels are plotted for contour lines of $|q^{[1]}|^2$ at height c^2 (on asymptotic plane), $c^2 + 1$, $c^2/2$ in order. There are fixed points located at (0,0.50) and (0, −0.50) in panel (a), (0,0.41) and (0, −0.41) in panel (b), (0,1.78) and (0,0.58), (0, −0.58), and (0, −1.78) in panel (c).

which has two asymptotes,

$$l_1 : x = (6 - 3a^2 - 6a)t, \quad l_2 : x = (6 - 3a^2 + 6a)t, \quad (31)$$

and two nonorthogonal axes,

$$\text{major axis} : t = 0, \quad \text{imaginary axis}(l_3) : x = (6 - 3a^2)t. \quad (32)$$

There are two fixed vertices—$P_1 = (0,0.50), P_2 = (0, -0.5)$—on the (t,x) plane of all values of a. Here l_3 is also a median of one triangle composed of above two asymptotes and a parallel line of the x axis except $t = 0$. We combine the density plots and the above three lines in Fig. 4 with different values of a. At height $c^2 + 1$, a contour line of $|q^{[1]|^2}$ with $c = 1$ is given by a quartic polynomial

$$\begin{aligned} &x^4 + (12a^2 - 24)tx^3 + \left[\tfrac{5}{2} + (216 - 144a^2 + 54a^4)t^2\right]x^2 \\ &+ [(-864 + 432a^2 - 216a^4 + 108a^6)t^3 \\ &+ (15a^2 - 30)t]x + (1296 + 648a^4 + 81a^8)t^4 \\ &+ \left[90 - 144a^2 + \left(\tfrac{45}{2}\right)a^4\right]t^2 - \tfrac{7}{16} = 0, \end{aligned} \quad (33)$$

which has two end points, $P_3 = [-\frac{\sqrt{7}}{12a}, \frac{(-2+a^2)\sqrt{7}}{4a}]$ and $P_4 = [\frac{\sqrt{7}}{12a}, -\frac{(-2+a^2)\sqrt{7}}{4a}]$, along the t direction. Moreover, there are two fixed points expressed by $P_5 = [0, \frac{\sqrt{-1-4c^2+4\sqrt{c^2(c^2+1)}}}{2c}|_{c=1}] = (0,0.41)$ and $P_6 = [0, -\frac{\sqrt{-1-4c^2+4\sqrt{c^2(c^2+1)}}}{2c}|_{c=1}] = (0, -0.41)$ on the (t,x) plane of all values of a. At height $\frac{c^2}{2}$, a contour line of $|q^{[1]}|^2$ with $c = 1$ is also given by a quartic polynomial

$$\begin{aligned} &x^4 + (12a^2 - 24)tx^3 + \left[(216 - 144a^2 + 54a^4)t^2 - \tfrac{7}{2}\right]x^2 \\ &+ [(-864 + 432a^2 - 216a^4 + 108a^6)t^3 \\ &+ (-21a^2 + 42)t]x + (1296 + 648a^4 + 81a^8)t^4 \\ &+ \left(-126 + 288a^2 - \tfrac{63}{2}a^4\right)t^2 + \tfrac{17}{16} = 0, \end{aligned} \quad (34)$$

which is defined on interval $[-\frac{1}{12a}, \frac{1}{12a}]$ of t. For this contour line, there are four fixed points—(0,1.78),(0,0.58),(0, −0.58),(0, −1.78)—on the (t,x) plane of all values of a. Two centers of valleys of $|q^{[1]}|^2$ are given by $P_7 = (0, \frac{\sqrt{3}}{2c}), P_8 = (0, -\frac{\sqrt{3}}{2c})$, which are independent

with the value of a. Figure 5 is plotted for above contour lines with different values of $a = 1.5, 2, 2.5$.

Based on the above analytical results, we could define the length and width of the RW, which are two crucial characters of a doubly localized wave-RW. Because the contour line of RW on the background plane is not a closed curve, we cannot define a length for RW on this plane. However, when we set d to be a positive constant, the contour line at height $c^2 + d$ is closed. Here $c^2 + d < 9c^2$ or, equivalently, $d < \sqrt{8c^2}$ because the max amplitude of the first-order RW ($|q^{[1]}|^2$) is $9c^2$. Without loss of generality, and considering a recognizable height from the asymptotic plane, we set $d = 1$ as before. We can use the length of the area surrounded by the contour line at height $c^2 + 1$ as the length of the first-order RW. The length direction is defined by l_3, the width direction is orthogonal to it. The reasons for this choice are (1) l_3 passes through P_3 and P_4; (2) l_3 is parallel to the tangent line of hyperbola at two vertices; (3) l_3 is parallel to the tangent line of the contour line at P_5 and P_6. Let k_3 be the slope of l_3. So the length of the first-order RW is the distance of P_3 and P_4, i.e.,

$$d_L = \frac{\sqrt{7}}{6a}\sqrt{1 + (k_3)^2} = \frac{\sqrt{7}}{6a}\sqrt{1 + (6 - 3a^2)^2}. \tag{35}$$

The width is defined as the projection of line segment P_7P_8 at width direction, which is expressed by

$$d_W = \frac{\sqrt{3}}{\sqrt{1 + (k_3)^2}} = \frac{\sqrt{3}}{\sqrt{1 + (6 - 3a^2)^2}}. \tag{36}$$

d_L and d_W are plotted in Fig. 6 with fixed $c = 1$, which shows that the length is decreased with a when $a \in (0, \sqrt{2})$ and is increased with a when $a > \sqrt{2}$. However, the width has an opposite increasing or decreasing trend with respect to a. When $a = \sqrt{2}$, the profile of first-order RW is parallel to the t axis, then the length reaches its minimum and the width reaches its maximum. This is the first role of a in the control of the RW. Moreover, we know from k_3 that the increase of a results in the rotation of RW in the clockwise direction. This is the second role of a.

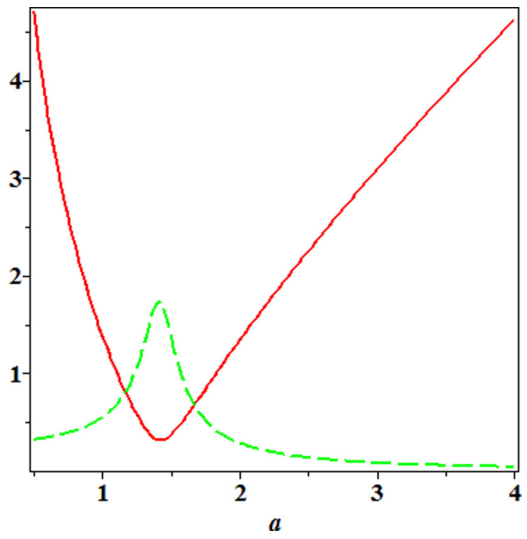

FIG. 6. (Color online) The length (red solid line) and the width (dashed green line) of the first-order RW $|q^{[1]}|^2$ with fixed $c = 1$. Note that $a = \sqrt{2}$ is an extreme point of d_L and d_W.

In above discussion for the role of a, we have set $c = 1$. If $c \neq 1$, it is a more interesting and complicated case, which can be studied as above by using contour line method. To save the space, we provide corresponding results without explanation, which can be done in a similar way as above. In this case, there are two asymptotes of the contour line of first-order RW $|q^{[1]}|^2$ at height c^2

$$\text{major axis} : t = 0, \quad \text{imaginary axis}(\text{cl}_3) : x = (6c^2 - 3a^2)t. \tag{37}$$

In other words, the slope is $k_{3c} = 6c^2 - 3a^2$. The two vertices of the hyperbola are $P_1 = (0, \frac{1}{2c})$ and $P_2 = (0, -\frac{1}{2c})$ on the (t,x) plane. For the contour line at height $c^2 + 1$, the two end points are $P_3 = [-\frac{\sqrt{8c^2-1}}{12ac^2}, \frac{(-2c^2+a^2)\sqrt{8c^2-1}}{4ac^2}]$ and $P_4 = [\frac{\sqrt{8c^2-1}}{12ac^2}, -\frac{(-2c^2+a^2)\sqrt{8c^2-1}}{4ac^2}]$ along the t direction. So the length of the first-order RW is

$$d_{cL} = \frac{\sqrt{8c^2 - 1}}{6c^2a}\sqrt{1 + 9(-2c^2 + a^2)^2}, \tag{38}$$

and the width of the first-order RW is

$$d_{cW} = \frac{\sqrt{3}}{c}\frac{1}{\sqrt{1 + 9(-2c^2 + a^2)^2}}, \tag{39}$$

which are plotted in Fig. 7. These plots show visually the role of a and c in the control of the first-order RW. For a given value of a, d_{cL} has two extreme points with respect to c. However, for a given value of c, d_{cL} has one extreme point with respect to a. The slope k_{3c} shows that the increasing of a and c results in the rotation of the first-order RW with different direction. Note that $a = \sqrt{2}c$ is a line of points for extreme value. Under this condition, the profile of first-order RW is parallel to the t axis, the minimum of the length is $\frac{\sqrt{4a^2-1}}{3a^3}$, and the maximum of the width is $\frac{\sqrt{3}}{c}$.

Triangular patterns. The triangular structure can be obtained by choosing the first nontrivial coefficient $s_1 \gg 1$, while the rest of the values are assumed to be zero. It can be seen from Figs. 8–10 that the nth-order rational solutions have $\frac{n(n+1)}{2}$ peaks of equal height with a structure of equilateral triangular type having n peaks at each edge.

Ring patterns. One can observe the ring structure or pattern when $n \geqslant 3$ and the principle coefficient for nth-order rational solution when $s_{n-1} \gg 1$, while the remaining coefficients s_i are all zero. The rational solutions consist of the outer circular shell of $2n - 1$ first-order rational solutions, while the center is an order $(n - 2)$ rational solution of the fundamental patterns as portrayed in Figs. 11 and 12. The center order-$(n - 2)$ RW can be decomposed further into different lower-order patterns according to the $(n - 2)$-reduction rule of order by setting one of s_i $(i = 0, 1, 2, \ldots, n - 3)$ to nonzero, which are plotted in Figs. 13–15. For example, the center order-4 RW of the sixth-order RW has a fundamental pattern [Fig. 12 (right)], a ring plus a fundamental pattern [Fig. 14 (right)], or a triangular pattern [Fig. 15 (right)] of second-order RW, a triangular pattern [Fig. 15 (left)]. We call these forms as standard decomposition of the RW.

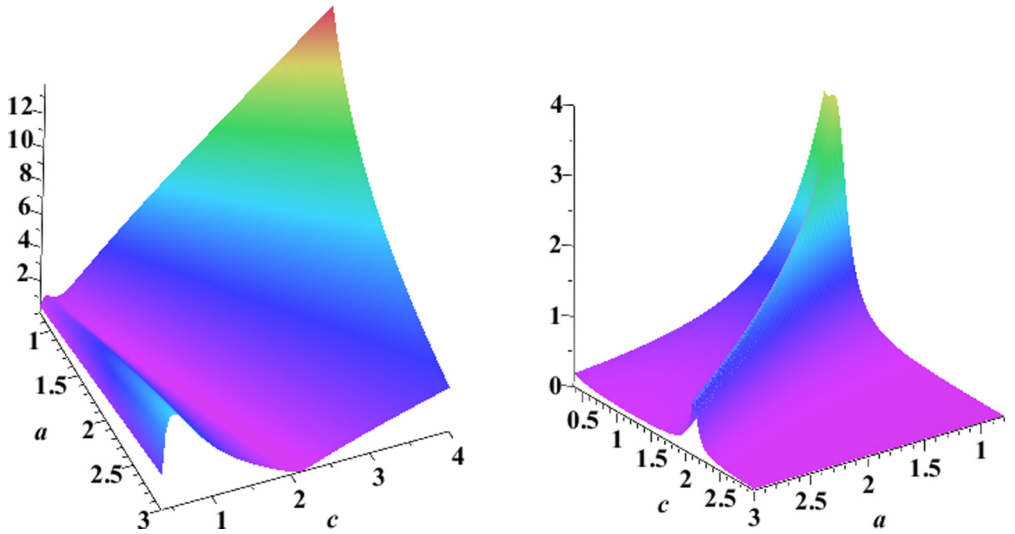

FIG. 7. (Color online) The length (left) and width (right) of the first-order RW $|q^{[1]}|^2$ with two parameters a and c.

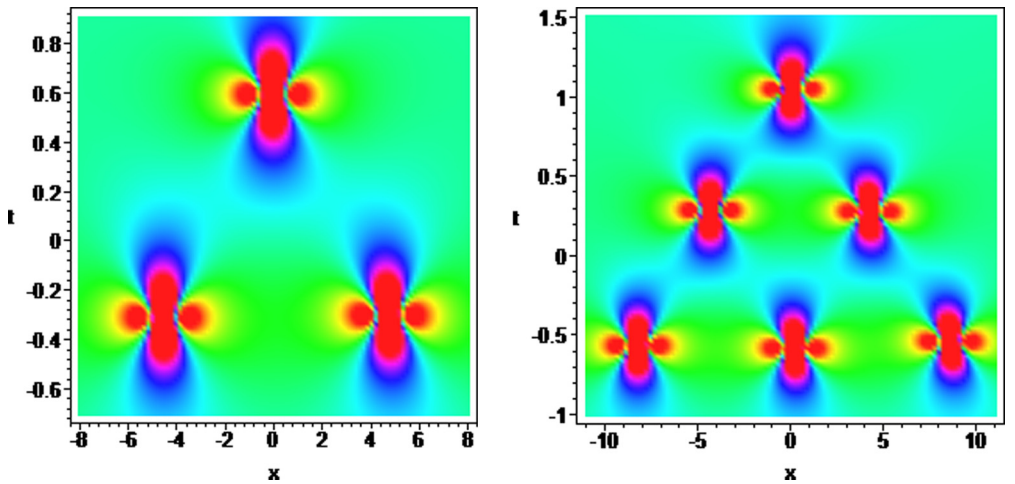

FIG. 8. (Color online) Triangular pattern of the second- and third-order RWs. The left panel is a density plot of $|q^{[2]}|^2$ (second-order RW), with $a = 1.44, c = 1, s_0 = 0, s_1 = 100$. The right panel is a density plot of $|q^{[3]}|^2$ (third-order RW), with $a = 1.44, c = 1, s_0 = 0, s_1 = 100, s_2 = 0$.

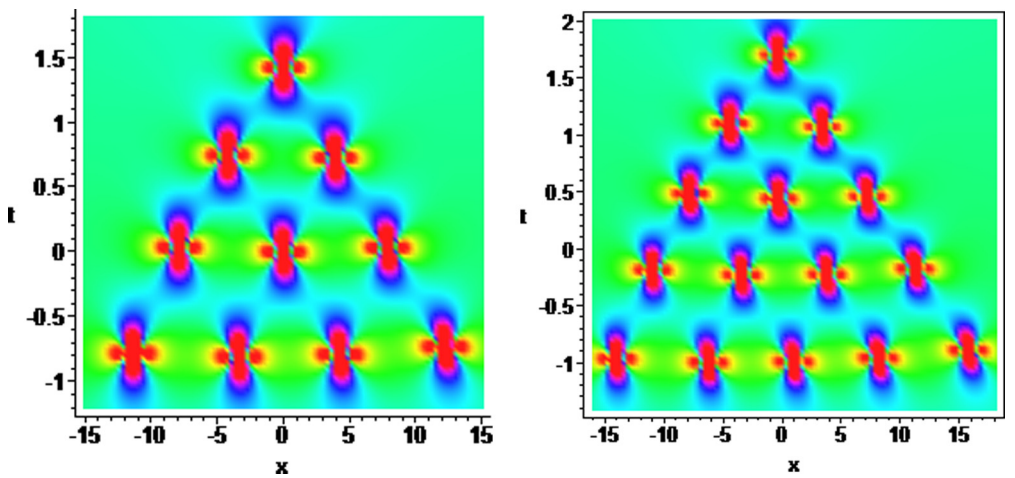

FIG. 9. (Color online) Triangular patterns of the fourth-order and fifth-order RWs. The left panel is a density plot of $|q^{[4]}|^2$ (fourth-order RW), with $a = 1.46, c = 1, s_0 = 0, s_1 = 100, s_2 = 0, s_3 = 0$; the right panel is a density plot of $|q^{[5]}|^2$ (fifth-order RW), with $a = 1.5, c = 1, s_0 = 0, s_1 = 100, s_2 = 0, s_3 = 0, s_4 = 0$.

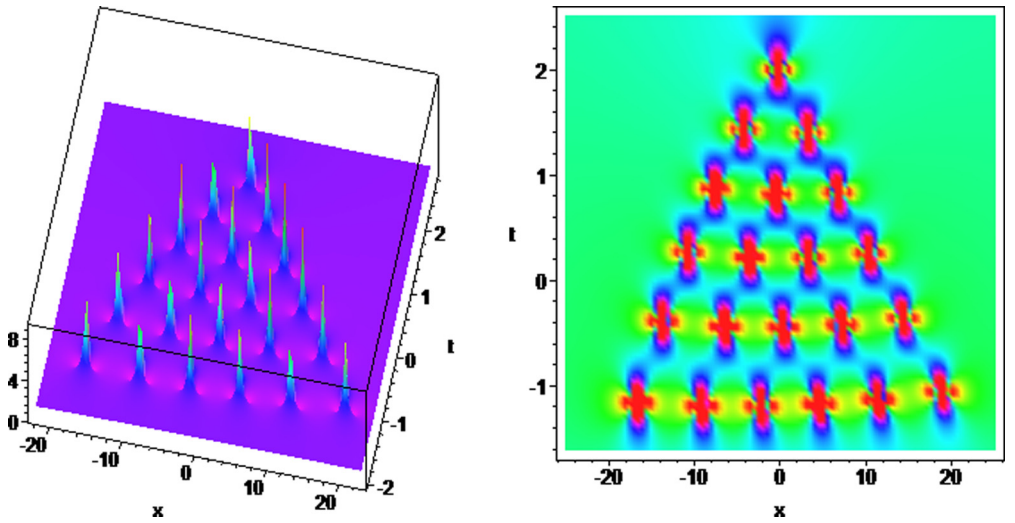

FIG. 10. (Color online) Triangular pattern of the sixth-order RW. The left panel is the evolution of $|q^{[6]}|^2$ (sixth-order RW) and the right panel is the corresponding density plot with $a = 1.5, c = 1, s_0 = 0, s_1 = 100, s_2 = 0, s_3 = 0, s_4 = 0, s_5 = 0$.

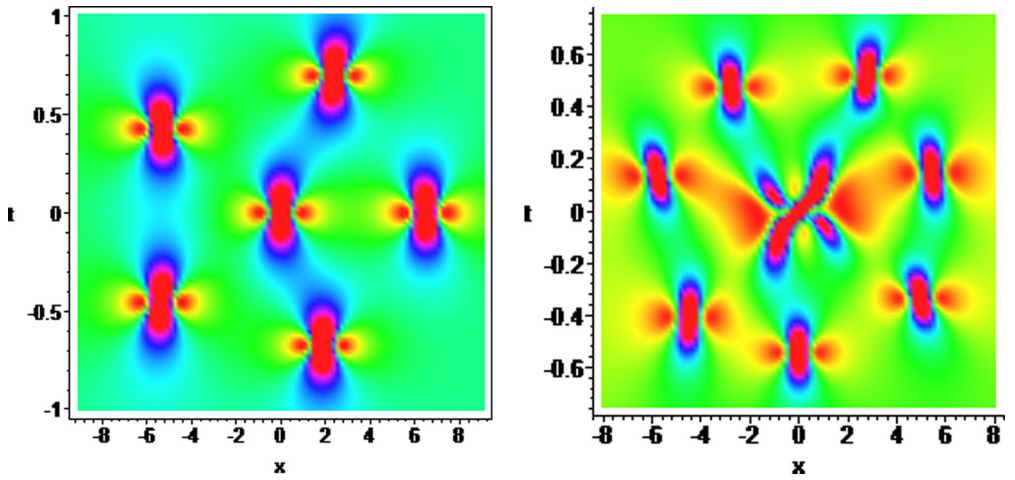

FIG. 11. (Color online) Standard circular decomposition of the RW: inner peak surrounded by ring pattern. The left panel is a density plot of $|q^{[3]}|^2$ (third-order RW) with $a = 1.4, c = 1, s_0 = 0, s_1 = 0, s_2 = 1000$; the right panel is a density plot of $|q^{[4]}|^2$ (fourth-order RW) with $a = 1.48, c = 1, s_0 = 0, s_1 = 0, s_2 = 0, s_3 = 1000$.

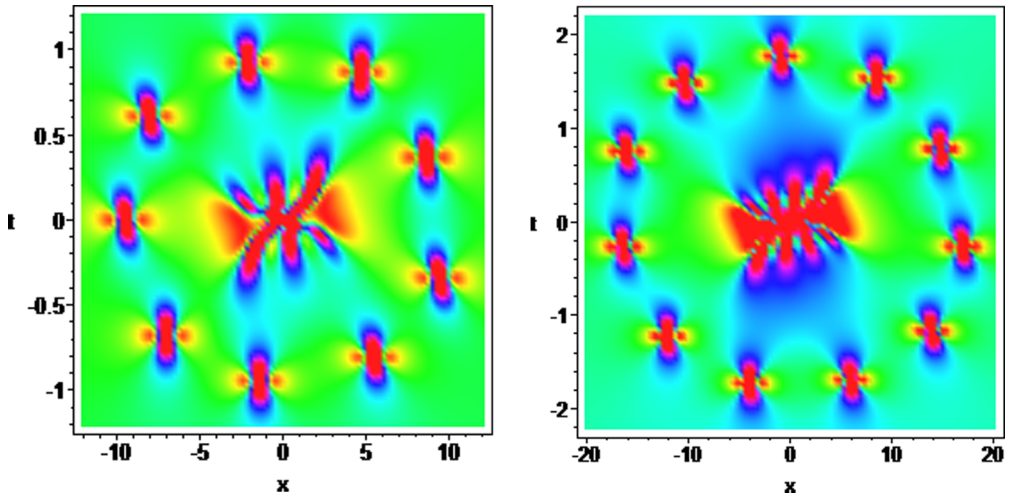

FIG. 12. (Color online) Standard circular decomposition of the RW: a ring pattern with inner third-order (left) and fourth-order (right) fundamental patterns. The left panel is a density plot of $|q^{[5]}|^2$ (fifth-order RW), with $a = 1.5, c = 1, s_0 = 0, s_1 = 0, s_2 = 0, s_3 = 0, s_4 = 100\,000$; the right panel is a density plot of $|q^{[6]}|^2$ (sixth-order RW), with $a = 1.5, c = 1, s_0 = 0, s_1 = 0, s_2 = 0, s_3 = 0, s_4 = 0, s_5 = 100\,000\,000$.

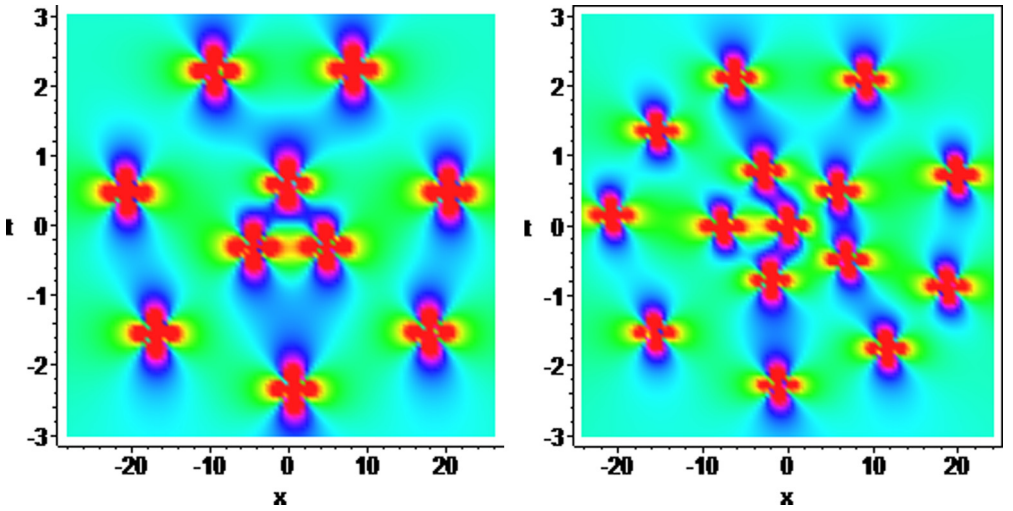

FIG. 13. (Color online) Standard circular decomposition of the fourth- and fifth-order RWs. The left panel is a density plot of $|q^{[4]}|^2$ (fourth-order RW), with $a = 1.45, c = 1, s_0 = 0, s_1 = 100, s_2 = 0, s_3 = 10\,000\,000$, which is decomposed into an outer ring with an inner second triangular pattern; the right panel is a density plot of $|q^{[5]}|^2$(fifth-order RW), with $a = 1.5, c = 1, s_0 = 0, s_1 = 100, s_2 = 0, s_3 = 500\,000, s_4 = 100\,000\,000$, which is decomposed into an inner peak surrounded by two rings.

This structure is similar to the so-called "wave clusters" as reported in [50].

Another interesting fact worth mentioning here is that the profiles of higher-order RW are actually a complicated combination of above three basic patterns—"fundamental" pattern, "ring" pattern, and "triangular" pattern—which can provide further interesting patterns of the RWs. This can be achieved by suitably selecting the different values of s_i. In particular, one can generate multiring structures but these rings do not possess $2n - 1$ peaks and also do not satisfy the rule of $(n - 2)$-reduction of order as mentioned earlier in the case of ring pattern formation. Thus, we call these formations nonstandard decomposition of the RWs. Figures 16–20 represent a few examples of this kind of special ring structures. One common feature, which we observed from these examples, is the appearance of at least two ring patterns with the same number of peaks. It should be noted that the centermost profile of Fig. 18 (left) is a fundamental pattern of a second-order RW, which clearly shows that Fig. 18 (left) is not a complete decomposition of the sixth-order RW. On the other hand, Fig. 18 (right) presents the complete decomposition. To arrive at a better understanding of the nonstandard decomposition, we provide the distribution of peaks in Table I. From Fig. 19 (left) the occurrence of two ring patterns with a single inner peak can also be observed; however, the inner ring consists of five triangular patterns. So the distribution of peaks is $5 + 3 \times 5 + 1$.

In spite of having different structures, all types of RW solutions possess a certain commonality as follows. The total number of peaks admitted by nth-order solutions is $\frac{n(n+1)}{2}$ in terms of a complete decomposition pattern. These structures actually depend on the choice of the free parameters. Among

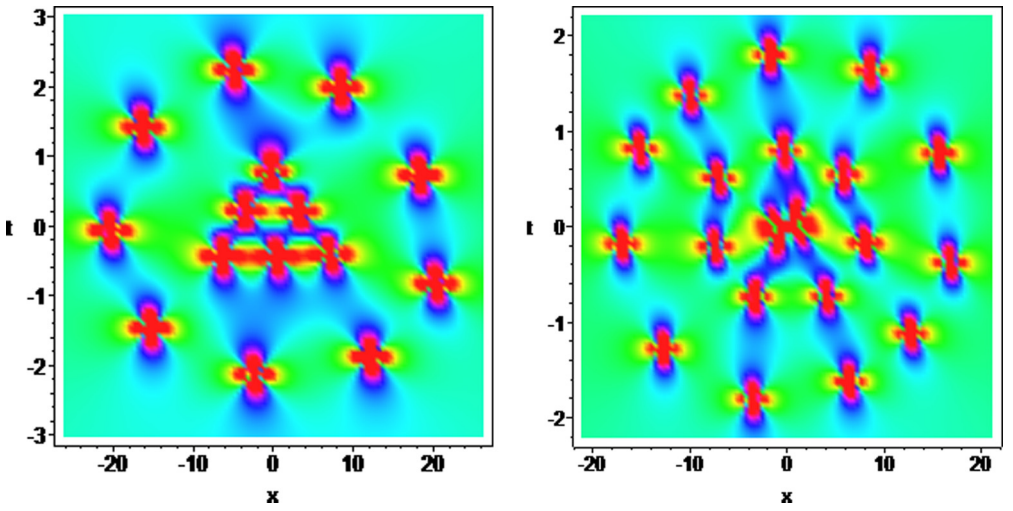

FIG. 14. (Color online) Standard circular decomposition of the fifth- and sixth-order RWs. The left panel is a density plot of $|q^{[5]}|^2$ (fifth-order RW), with $a = 1.5, c = 1, s_0 = 0, s_1 = 50, s_2 = 0, s_3 = 0, s_4 = 100\,000\,000$, which is decomposed into a ring pattern with an inner third triangular pattern; the right panel is a density plot of $|q^{[6]}|^2$ (sixth-order RW), with $a = 1.5, c = 1, s_0 = 0, s_1 = 0, s_2 = 0, s_3 = 0, s_4 = 1\,000\,000, s_5 = 100\,000\,000$, which is decomposed into two ring patterns plus an inner second fundamental pattern.

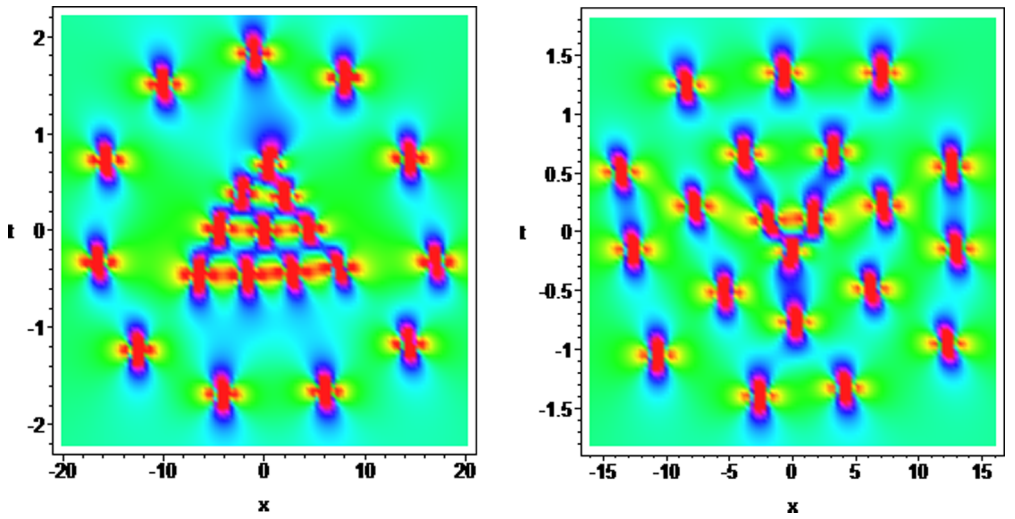

FIG. 15. (Color online) Standard circular decomposition of the sixth-order RW. The left panel is a density plot of $|q^{[6]}|^2$ (sixth-order RW), with $a = 1.5, c = 1, s_0 = 0, s_1 = 18, s_2 = 0, s_3 = 0, s_4 = 0, s_5 = 100\,000\,000$, which is decomposed into a ring plus an inner fourth-order triangular pattern; the right panel is a density plot of $|q^{[6]}|^2$ (sixth-order RW), with $a = 1.5, c = 1, s_0 = 0, s_1 = 0, s_2 = 0, s_3 = 7000, s_4 = 0, s_5 = 10\,000\,000$ which is decomposed into three rings.

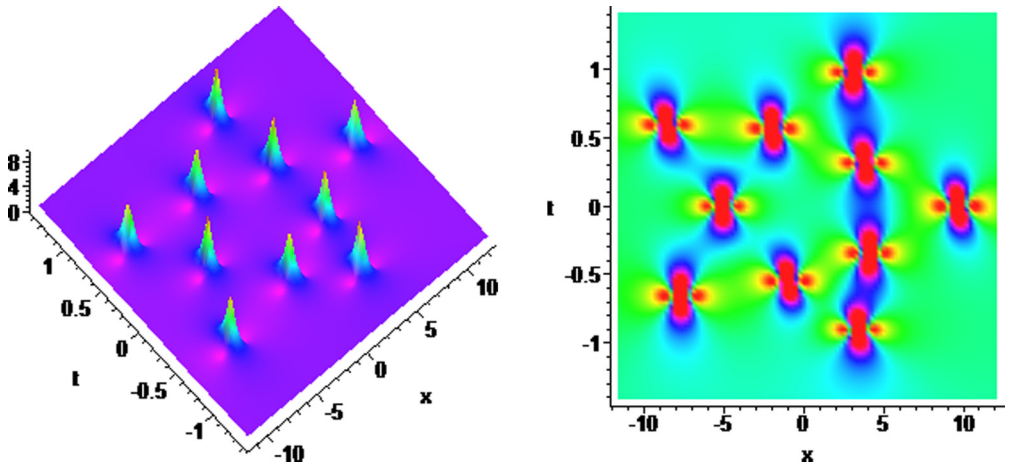

FIG. 16. (Color online) Nonstandard circular decomposition of the fourth-order RW: two rings. The left panel is the dynamical evolution of $|q^{[4]}|^2$ (fourth-order RW) and the right panel is the corresponding density plot with $a = 1.48, c = 1, s_0 = 0, s_1 = 0, s_2 = 1000, s_3 = 0$.

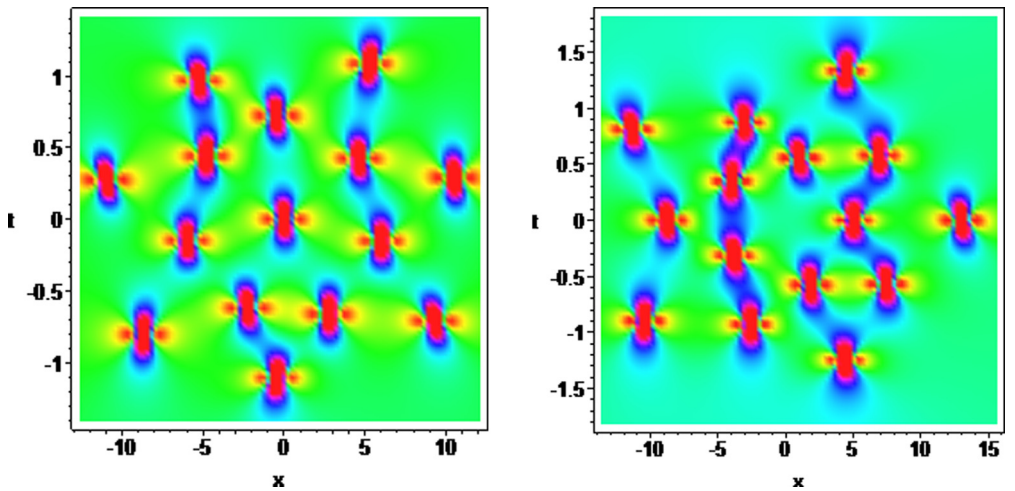

FIG. 17. (Color online) Nonstandard circular decomposition of the fifth-order RWs: two rings plus an inner peak (left) and three rings (right). The left panel is a density plot of $|q^{[5]}|^2$ (fifth-order RW), with $a = 1.45, c = 1, s_0 = 0, s_1 = 0, s_2 = 0, s_3 = 10\,000, s_4 = 0$; the right panel is a density plot of $|q^{[5]}|^2$ (fifth-order RW), with $a = 1.46, c = 1, s_0 = 0, s_1 = 0, s_2 = 1000, s_3 = 0, s_4 = 0$.

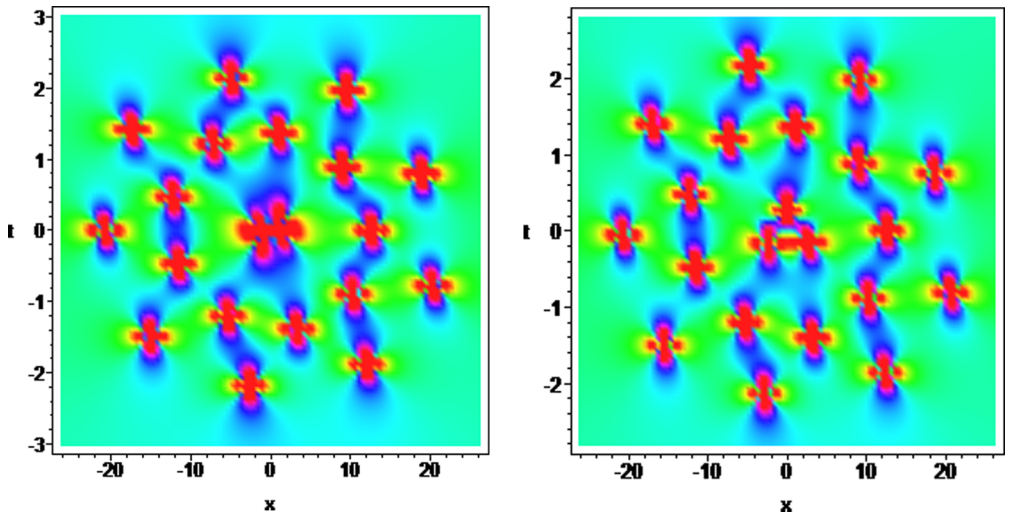

FIG. 18. (Color online) Nonstandard circular decomposition of the sixth-order RW: two ring patterns with an inner second fundamental pattern (left) and three rings (right). The left panel is a density plot of $|q^{[6]}|^2$ (sixth-order RW), with $a = 1.5, c = 1, s_0 = 0, s_1 = 0, s_2 = 0, s_3 = 0, s_4 = 10\,000\,000, s_5 = 0$; the right panel is a density plot of $|q^{[6]}|^2$ (sixth-order RW), with $a = 1.5, c = 1, s_0 = 0, s_1 = 15, s_2 = 0, s_3 = 0, s_4 = 10\,000\,000, s_5 = 0$.

all parameters, the principle coefficient s_{n-1} is accountable for the formation of a ring structure. The first nontrivial coefficient s_1 is responsible for the evolution of a triangular structure. Furthermore, to see the difference between the RWs of the complex mKdV and the NLS clearly, we use the first-order RW [40] of the NLS, i.e.,

$$q^{[1]}_{\mathrm{NLS}} = c^2 \frac{\tilde{A} - 32c^2[(-x+2at)^2 - 4c^2t^2] + 8}{\tilde{A}}, \qquad \tilde{A} = [4c^2x^2 - 16c^2xta + 16t^2(c^4 + c^2a^2) + 1]^2, \tag{40}$$

to calculate the contour lines at heights c^2 and $c^2 + 1$, and to calculate the length and width by the same procedure we have used in complex mKdV. Here the NLS equation is in the form of

$$iq_t + q_{xx} + 2|q^2|q = 0. \tag{41}$$

Similar to the contour line method of the complex mKdV, we get the slope of the imaginary axis of the hyperbola formed by a contour line of the $|q^{[1]}_{\mathrm{NLS}}|^2$ on the background plane with a height c^2:$k_{3c\mathrm{NLS}} = 2a$, the length of the RW

$$d_{cL\mathrm{NLS}} = \frac{1}{2c^2}\sqrt{(-1+8c^2)(1+4a^2)}, \tag{42}$$

and the width of the RW

$$d_{cW\mathrm{NLS}} = \frac{\sqrt{3}}{c\sqrt{1+4a^2}}. \tag{43}$$

The dynamical evolution of the first-order RW $|q^{[1]}_{\mathrm{NLS}}|^2$ of the NLS is plotted in Fig. 21; contour lines at heights c^2 and $c^2 + 1$ of the first-order RWs of the complex mKdV and the NLS are plotted in Fig. 22. These pictures and analytical formulas of length and width show that, for the first-order RWs of the

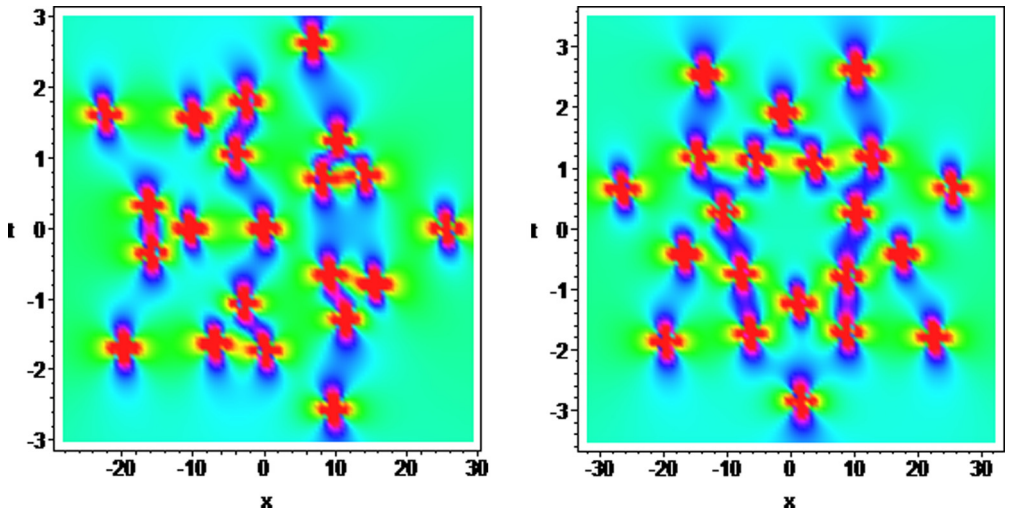

FIG. 19. (Color online) Nonstandard circular decomposition of the sixth-order RW: three rings plus an inner peak (left) and three rings (right). The left panel is a density plot of $|q^{[6]}|^2$ (sixth-order RW), with $a = 1.5, c = 1, s_0 = 0, s_1 = 0, s_2 = 10\,000, s_3 = 0, s_4 = 0, s_5 = 0$; the right panel is a density plot of $|q^{[6]}|^2$ (sixth-order RW), with $a = 1.5, c = 1, s_0 = 0, s_1 = 0, s_2 = 0, s_3 = 1\,000\,000, s_4 = 0, s_5 = 100\,000\,000$.

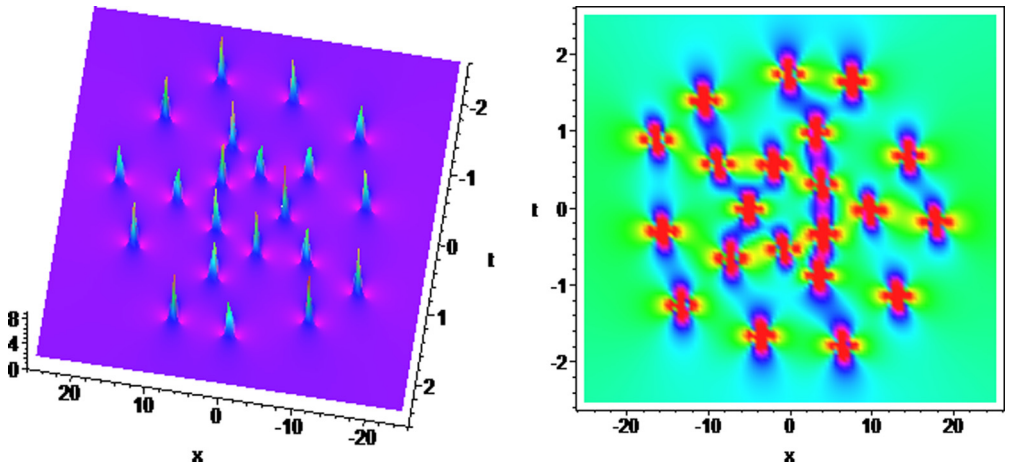

FIG. 20. (Color online) Nonstandard circular decomposition of the sixth-order RW: three rings. The left panel is the dynamical evolution of $|q^{[6]}|^2$ (sixth-order RW) and the right panel is the corresponding density plot with $a = 1.5, c = 1, s_0 = 0, s_1 = 0, s_2 = 1000, s_3 = 1\,000\,000, s_4 = 0, s_5 = 100\,000\,000$.

complex mKdV and the NLS, they are very similar to each other apart from a remarkable tilt with respect to the axes and a remarkable shortening of length of them with the same values of a and c. In other words, the inclusion of third-order dispersion and time-delay correction is responsible for a strong rotation and a strong compression effects in the first-order RW of the complex mKdV equation. In particular, if $a = 0$, $|q^{[1]}_{\rm NLS}|2$ is still a RW, but $|q^{[1]}|^2$ of the complex mKdV is a soliton traveling along l_3 which is no longer doubly localized in x and t directions.

In terms of applications, the investigation of the above investigated higher-order RW solutions will be useful to understand the generation of high-power waves and their possible splitting, etc. As we have discussed earlier, very recently, using the non-slowly varying envelope approximation (SVEA), the complex mKdV equation has been derived and the generation of few-cycle optical pulses have been reported [42,43]. In addition, it has been pointed out that these types of few-cycle optical pulses require no phase matching (a main issue in nonlinear optics), which makes a strong contrast and provides an interesting aspect when compared with the longer pulses derived by using the SVEA method. From these recent studies it is also interesting to note that these types of few-cycle optical pulses are very similar to the generation of high-power and very short RW-type ultrashort pulses. For example, in nonlinear photonic crystal fiber, the above waves may be connected to the generation of few-cycle optical pulses which will be useful to realize the so-called SCG. This type of white light continuum coherence source will find a range of applications in optical coherence tomography, optical meteorology, wavelength division multiplexing, fluorescence microscopy, flow cytometry, atmospheric sensing, etc.[1,42,43].

V. CONCLUSIONS

In this paper, we applied the DT to construct the higher-order RW-type rational solutions as well as the evolution of RWs for the complex mKdV equation. Based on detailed numerical and analytical investigations, we classified the higher-order RWs with respect to their intrinsic structure. We use the contour line method to define the length and width of the first-order RW and then provide their analytical formulas related to two parameters a and c. We illustrate clearly, by analytical formulas and figures, that the differences between the first-order RWs of the mKdV and the NLS are mainly due to strong rotation, as well as strong compression effects. Furthermore, we observed that there are three principle types, namely, fundamental pattern, ring pattern, and triangular pattern. The composition of these three principle patterns is mainly because of higher-order RWs. We also provided several further new patterns of the higher-order RWs of this model. The ring patterns obtained in this paper are similar to the "atom" structure reported in [50]. This explains the generalization and evolution of higher-order RWs in terms of the solution. On the other hand, by changing the free parameters in the DT, we have also constructed more complicated (and interesting) structures. We deduced from our stimulated examples in Figs. 16–20 that the nonstandard decomposition deserves further studies because there are presently unknown rules of the decomposition. Applying our construction of RW solutions to different completely integrable NEEs, it is interesting to investigate some analogs between the evolution and decomposition of

TABLE I. Distribution of peaks on rings by non-standard decomposition,

Order	Distributions of peaks on rings (L, left; R, right)			
4	5 + 5 (Fig. 12)			
5	7 + 7 + 1 (Fig. 13L)	5 + 5 + 5 (Fig. 13R)		
6	9 + 9 + 3 (Fig. 14R)	5 + 10 + 5 + 1 (Fig. 15L)	7 + 7 + 7 (Fig. 15R)	11 + 5 + 5 (Fig. 16)

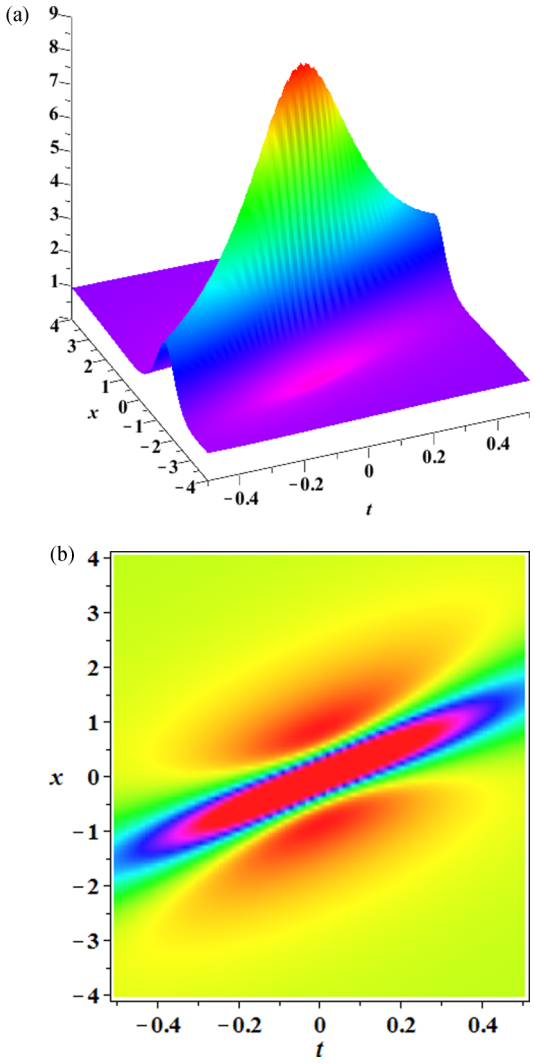

FIG. 21. (Color online) The first-order RW ($|q^{[1]}_{\rm NLS}|^2$) of the NLS with $a = 1.5$ and $c = 1$. Panel (a) is the dynamical evolution of $|q^{[1]}_{\rm NLS}|^2$ and the panel (b) is the corresponding density plot.

higher-order RWs of these different integrable equations. It is essential to find further conserved quantities for the kind of solutions. These studies may help us for better understanding of the occurrence of deep ocean waves with large amplitude as well as the generation of few-cycle optical pulses emitted by high-power lasers which are used for the recently invented SCG sources, etc.

If we compare our results with the work in [38] on the RW solutions of the complex mKdV, our results have following advantages and developments.

(i) Our method is considerably simpler as well as more systematic. From Theorem 3, one can directly obtain the higher-order RWs without calculating eigenfunctions $\psi_1^{[i]}$ and $\phi_1^{[i]}(i = 0,1,2,3)$ as in [38].

(ii) We applied the contour line method to find the analytical description of the length and width of the first-order RW of the complex mKdV and the NLS equation. We illustrated clearly, using suitable analytical formulae and figures, that the differences between the first-order RWs of the mKdV and the NLS are due to a strong rotation and a strong compression effects. Note that, setting $a = 0$, $|q^{[1]}|^2$ reduces to a soliton on a background plane at height c^2, but $|q^{[1]}_{\rm NLS}|^2$ cannot.

(iii) We proposed and proved a convenient way to control the patterns and evolutions of the RW by standard and nonstandard decomposition with suitable choices of s_i.

(iv) We generated interesting patterns for fourth-, fifth-, and sixth-order RWs.

With respect to the future research in this exciting area, we shall apply the contour line method to the first-order RW of the different NLS-type equations. For the higher-order RWs, because the degree of polynomials in its explicit form is more than 4, it is not easy to get the analytical expressions of the asymptotes for its contour lines in general. Thus, how to get the analytical results on their length and width is an interesting, difficult, and important problem, which deserves further study.

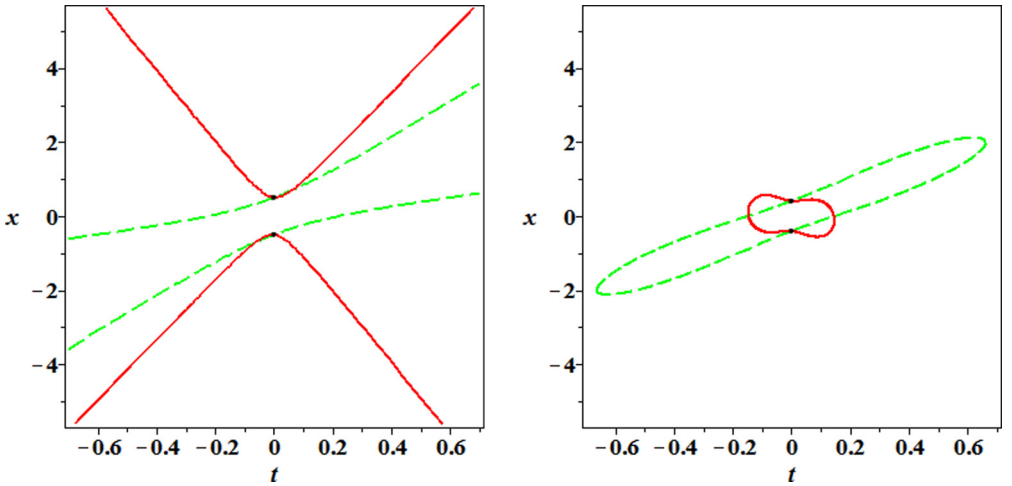

FIG. 22. (Color online) Contour lines of the first-order RW of the complex mKdV ($|q^{[1]}|^2$, red solid lines) and NLS ($|q^{[1]}_{\rm NLS}|^2$, green dashed lines), with $a = 1.5$ and $c = 1$. The left panel is plotted at height c^2 (on the asymptotical plane); the right panel is plotted at height $c^2 + 1$. Two lines have two common pints: (0,0.50),(0, −0.50) in the left panel and (0,0.41),(0, − 0.41) in the right panel.

ACKNOWLEDGMENTS

This work is supported by the NSF of China under Grant No. 11271210 and the K. C. Wong Magna Fund in Ningbo University. J.S.H. thanks sincerely Professor A. S. Fokas for arranging a visit to Cambridge University and for many useful discussions. K.P. acknowledges DST, NBHM, CSIR, and IFCPAR, Government of India, for the financial support through major projects. R.E. acknowledges M. Kéray for advice and is also grateful to NSF, Hungary (OTKA, Ref. No. K83133). This work has been partially supported by The University of Sheffield's MSRC Visitor Grant.

APPENDIX A

In Eq. (28), L_1 are L_2 are given by

$$\begin{aligned}B :=\ & 2\,239\,488a^4c^{14}t^6 + 46\,656a^{12}c^6t^6 + 2\,985\,984c^{18}t^6 + 559\,872a^8c^{10}t^6 + 746\,496a^6c^{10}t^5x + 93\,312a^{10}c^6t^5x \\ & - 1\,492\,992a^4c^{12}t^5x - 186\,624a^8c^8t^5x + 1492\,992a^2c^{14}t^5x - 2\,985\,984c^{16}t^5x + 1\,244\,160c^{14}t^4x^2 - 248\,832a^6c^8t^4x^2 \\ & - 995\,328a^2c^{12}t^4x^2 + 622\,080a^4c^{10}t^4x^2 + 77\,760a^8c^6t^4x^2 - 276\,480c^{12}t^3x^3 + 34\,560a^6c^6t^3x^3 - 124\,416a^4c^8t^3x^3 \\ & + 248\,832a^2c^{10}t^3x^3 + 34\,560c^{10}t^2x^4 + 8640a^4c^6t^2x^4 - 27\,648a^2c^8t^2x^4 + 1152a^2c^6tx^5 - 2304c^8tx^5 + 64c^6x^6 \\ & - 331\,776c^6a^6t^4 - 518\,400c^{12}t^4 + 155\,520c^8a^4t^4 - 11\,664c^4a^8t^4 + 290\,304c^{10}t^3x - 15\,552c^4a^6t^3x + 103\,680c^8a^2t^3x \\ & - 176\,256c^6a^4t^3x - 58\,752c^8t^2x^2 - 6912c^6a^2t^2x^2 - 7776c^4a^4t^2x^2 + 4992c^6tx^3 - 1728c^4a^2tx^3 - 144c^4x^4 \\ & + 124\,416ac^{10}s_1t^3 + 31\,104a^5c^6s_1t^3 - 165\,888a^3c^8s_1t^3 + 20\,736a^3c^6s_1t^2x - 41\,472ac^8s_1t^2x + 3456ac^6s_1tx^2 \\ & - 18\,000c^6t^2 - 1620c^2a^4t^2 - 1080c^2a^2tx + 5\,616c^4tx - 180c^2x^2 + 864c^4as_1t + 144c^4s_1^2 + 45 + i(2\,985\,984ac^{14}t^5 \\ & + 1\,492\,992a^5c^{10}t^5 + 186\,624a^9c^6t^5 - 497\,664a^5c^8t^4x + 995\,328a^3c^{10}t^4x - 1\,990\,656ac^{12}t^4x + 248\,832a^7c^6t^4x \\ & - 331\,776a^3c^8t^3x^2 + 124\,416a^5c^6t^3x^2 + 497\,664ac^{10}t^3x^2 - 55\,296ac^8t^2x^3 + 27\,648a^3c^6t^2x^3 + 2304ac^6tx^4 \\ & + 207\,360c^8at^3 - 31\,104c^4a^5t^3 - 13\,824c^6at^2x - 20\,736c^4a^3t^2x - 3456c^4atx^2 + 20\,736c^8s_1t^2 - 41\,472a^2c^6s_1t^2 \\ & + 5184a^4c^4s_1t^2 + 3456a^2c^4s_1tx - 6912c^6s_1tx + 576c^4s_1x^2 - 2\,160ac^2t + 144s_1c^2)\end{aligned}$$

and

$$\begin{aligned}C :=\ & 2\,239\,488a^4c^{14}t^6 + 2\,985\,984c^{18}t^6 + 46\,656a^{12}c^6t^6 + 559\,872a^8c^{10}t^6 + 746\,496a^6c^{10}t^5x - 1\,492\,992a^4c^{12}t^5x \\ & - 186\,624a^8c^8t^5x - 2\,985\,984c^{16}t^5x + 93\,312a^{10}c^6t^5x + 1\,492\,992a^2c^{14}t^5x + 1\,244\,160c^{14}t^4x^2 - 995\,328a^2c^{12}t^4x^2 \\ & + 622\,080a^4c^{10}t^4x^2 + 77\,760a^8c^6t^4x^2 - 248\,832a^6c^8t^4x^2 + 248\,832a^2c^{10}t^3x^3 + 34\,560a^6c^6t^3x^3 - 124\,416a^4c^8t^3x^3 \\ & - 276\,480c^{12}t^3x^3 - 27\,648a^2c^8t^2x^4 + 8640a^4c^6t^2x^4 + 34\,560c^{10}t^2x^4 - 2304c^8tx^5 + 1\,152a^2c^6tx^5 + 64c^6x^6 \\ & + 995\,328c^{10}a^2t^4 + 279\,936c^8a^4t^4 - 82\,944c^6a^6t^4 + 3888c^4a^8t^4 - 269\,568c^{12}t^4 + 124\,416c^{10}t^3x + 5184c^4a^6t^3x \\ & - 51\,840c^6a^4t^3x - 145\,152c^8a^2t^3x - 17\,280c^8t^2x^2 - 6912c^6a^2t^2x^2 + 2592c^4a^4t^2x^2 + 384c^6tx^3 + 576c^4a^2tx^3 \\ & + 48c^4x^4 - 165\,888a^3c^8s_1t^3 + 124\,416ac^{10}s_1t^3 + 31\,104a^5c^6s_1t^3 + 20\,736a^3c^6s_1t^2x - 41\,472ac^8s_1t^2x + 3456ac^6s_1tx^2 \\ & + 20\,016c^6t^2 + 972c^2a^4t^2 + 6912c^4a^2t^2 + 648c^2a^2tx - 2448c^4tx + 108c^2x^2 - 2592c^4as_1t + 144c^4s_1^2 + 9.\end{aligned}$$

APPENDIX B

In Eq. (29), L_1 are L_2 are given by

$$\begin{aligned}L_1 :=\ & -4\,939\,273\,445\,868\,140\,625t^{12} - 545\,023\,276\,785\,450\,000t^{11}x - 388\,407\,392\,651\,700\,000t^{10}x^2 \\ & - 34\,025\,850\,934\,560\,000t^9x^3 - 12\,374\,529\,519\,456\,000t^8x^4 - 841\,946\,352\,721\,920t^7x^5 \\ & - 204\,871\,837\,925\,376t^6x^6 - 10\,322\,713\,903\,104t^5x^7 - 1\,860\,148\,592\,640t^4x^8 - 62\,710\,087\,680t^3x^9 \\ & - 8\,776\,581\,120t^2x^{10} - 150\,994\,944tx^{11} - 16\,777\,216x^{12} + 2\,300\,237\,292\,280\,725\,000t^{10} \\ & + 500\,080\,291\,038\,360\,000t^9x + 178\,207\,653\,254\,544\,000t^8x^2 + 20\,160\,748\,631\,347\,200t^7x^3 \\ & + 4\,231\,975\,119\,851\,520t^6x^4 + 253\,682\,249\,269\,248t^5x^5 + 40\,317\,552\,230\,400t^4x^6 + 880\,347\,709\,440t^3x^7 \\ & + 141\,203\,865\,600t^2x^8 - 1\,447\,034\,880tx^9 + 75\,497\,472x^{10} + 257\,120\,426\,548\,112\,400t^8 \\ & - 88\,521\,031\,030\,049\,280t^7x - 1\,841\,385\,225\,323\,520t^6x^2 - 617\,799\,343\,104\,000t^5x^3 \\ & - 88\,747\,774\,156\,800t^4x^4 - 8\,252\,622\,766\,080t^3x^5 - 200\,693\,514\,240t^2x^6 + 1\,415\,577\,600tx^7 \\ & + 235\,929\,600x^8 + 12\,647\,412\,412\,496\,640t^6 + 42\,148\,769\,126\,400t^5x - 2\,996\,161\,228\,800t^4x^2\end{aligned}$$

$$
\begin{aligned}
&- 15\,902\,996\,889\,600t^3x^3 + 313\,860\,096\,000t^2x^4 - 8\,139\,571\,200tx^5 + 707\,788\,800x^6 \\
&- 149\,676\,507\,590\,400t^4 + 2\,148\,738\,969\,600t^3x - 1\,622\,998\,425\,600t^2x^2 + 31\,186\,944\,000t^3x \\
&- 928\,972\,800x^4 - 95\,215\,564\,800t^2 + 21\,598\,617\,600tx - 464\,486\,400x^2 + 58\,060\,800 \\
&+ i(-6\,540\,279\,321\,425\,400\,000t^{11} - 601\,404\,995\,073\,600\,000t^{10}x - 423\,057\,306\,879\,360\,000t^9x^2 \\
&- 29\,901\,007\,761\,408\,000t^8x^3 - 10\,648\,770\,814\,771\,200t^7x^4 - 552\,411\,244\,265\,472t^6x^5 \\
&- 130\,559\,642\,173\,440t^5x^6 - 4\,494\,741\,995\,520t^4x^7 - 779\,700\,142\,080t^3x^8 - 13\,589\,544\,960t^2x^9 \\
&- 1\,811\,939\,328tx^{10} - 303\,419\,904\,173\,280\,000t^9 + 263\,517\,097\,430\,016\,000t^8x \\
&+ 29\,562\,711\,599\,923\,200t^7x^2 + 7\,820\,253\,397\,647\,360t^6x^3 + 799\,710\,056\,939\,520t^5x^4 \\
&+ 58\,500\,443\,013\,120t^4x^5 + 5\,243\,865\,661\,440t^3x^6 + 40\,768\,634\,880t^2x^7 + 6\,794\,772\,480tx^8 \\
&+ 10\,822\,374\,648\,023\,040t^7 - 15\,805\,156\,998\,758\,400t^6x - 366\,298\,181\,959\,680t^5x^2 \\
&+ 157\,459\,297\,075\,200t^4x^3 - 6\,736\,379\,904\,000t^3x^4 - 249\,707\,888\,640t^2x^5 + 16\,986\,931\,200tx^6 \\
&+ 2\,321\,279\,745\,269\,760t^5 - 164\,322\,282\,700\,800t^4x + 7\,849\,554\,739\,200t^3x^2 - 700\,710\,912\,000t^2x^3 \\
&+ 38\,220\,595\,200tx^4 + 4\,992\,863\,846\,400t^3 - 967\,458\,816\,000t^2x - 33\,443\,020\,800tx^2 - 8\,360\,755\,200t) \\
L_2 := &\, 4\,939\,273\,445\,868\,140\,625t^{12} + 545\,023\,276\,785\,450\,000t^{11}x + 388\,407\,392\,651\,700\,000t^{10}x^2 \\
&+ 34\,025\,850\,934\,560\,000t^9x^3 + 12\,374\,529\,519\,456\,000t^8x^4 + 841\,946\,352\,721\,920t^7x^5 \\
&+ 204\,871\,837\,925\,376t^6x^6 + 10\,322\,713\,903\,104t^5x^7 + 1\,860\,148\,592\,640t^4x^8 \\
&+ 62\,710\,087\,680t^3x^9 + 8\,776\,581\,120t^2x^{10} + 150\,994\,944tx^{11} + 16\,777\,216x^{12} \\
&+ 1\,671\,541\,529\,351\,175\,000t^{10} - 201\,221\,180\,459\,640\,000t^9x + 29\,583\,374\,214\,960\,000t^8x^2 \\
&- 8\,646\,206\,984\,294\,400t^7x^3 - 205\,872\,145\,551\,360t^6x^4 - 102\,185\,078\,390\,784t^5x^5 \\
&- 5\,361\,951\,375\,360t^4x^6 - 141\,416\,202\,240t^3x^7 - 16\,349\,921\,280t^2x^8 + 2\,202\,009\,600tx^9 \\
&+ 25\,165\,824x^{10} + 214\,192\,109\,547\,903\,600t^8 + 4\,346\,367\,735\,790\,080t^7x \\
&+ 3\,783\,154\,346\,910\,720t^6x^2 - 1\,075\,635\,551\,969\,280t^5x^3 + 40\,942\,170\,316\,800t^4x^4 \\
&+ 1\,840\,480\,911\,360t^3x^5 + 84\,333\,035\,520t^2x^6 + 849\,346\,560tx^7 + 141\,557\,760x^8 \\
&+ 3\,537\,485\,306\,138\,880t^6 + 789\,853\,361\,080\,320t^5x + 130\,057\,245\,388\,800t^4x^2 \\
&- 11\,222\,478\,028\,800t^3x^3 + 402\,245\,222\,400t^2x^4 - 4\,034\,396\,160tx^5 + 613\,416\,960x^6 \\
&+ 90\,779\,142\,700\,800t^4 - 6\,216\,180\,019\,200t^3x - 269\,186\,457\,600t^2x^2 + 11\,988\,172\,800tx^3 \\
&+ 221\,184\,000x^4 + 213\,178\,521\,600t^2 - 5\,009\,817\,600tx + 199\,065\,600x^2 + 8\,294\,400.
\end{aligned}
$$

[1] G. P. Agrawal, *Nonlinear Fiber Optics*, 5th ed. (Academic Press, San Diego, 2012).

[2] B. A. Malomed, *Soliton Management in Periodic Systems* (Springer, New York, 2006).

[3] S. K. Turitsyn, B. G. Bale, and M. P. Fedoruk, Phys. Report **521**, 135 (2012).

[4] D. J. Korteweg and G. de Vries, Philos. Mag. **39**, 422 (1895).

[5] N. J. Zabusky and M. D. Kruskal, Phys. Rev. Lett. **15**, 240 (1965).

[6] V. E. Zakharov and A. B. Shabat, Sov. Phys. JETP **34**, 62 (1972).

[7] L. F. Mollenauer, R. H. Stolen, and J. P. Gordon, Phys. Rev. Lett. **45**, 1095 (1980).

[8] A. Hasegawa and F. D. Tappert, Appl. Phys. Lett. **23**, 142 (1973).

[9] D. H. Peregrine, J. Aust. Math. Soc. B **25**, 16 (1983).

[10] D. R. Solli, C. Ropers, P. Koonath, and B. Jalali, Nature (London) **450**, 1054 (2007).

[11] D. R. Solli, C. Ropers, and B. Jalali, Phys. Rev. Lett. **101**, 233902 (2008).

[12] J. M. Dudley, G. Genty and S. Coen, Rev. Mod. Phys. **78**, 1135 (2006); J. M. Dudley, G. Genty, F. Dias, B. Kibler, and N. Akhmediev, Opt. Express **17**, 21497 (2009).

[13] A. N. Ganshin, V. B. Efimov, G. V. Kolmakov, L. P. Mezhov-Deglin, and P. V. E. McClintock, Phys. Rev. Lett. **101**, 065303 (2008).

[14] Yu. V. Bludov, V. V. Konotop, and N. Akhmediev, Phys. Rev. A **80**, 033610 (2009).

[15] M. S. Ruderman, Eur. Phys. J. Spec. Top. **185**, 57 (2010).

[16] W. M. Moslem, P. K. Shukla, and B. Eliasson, EuroPhys. **96**, 25002 (2011).

[17] R. Höhmann, U. Kuhl, H.-J. Stöckmann, L. Kaplan, and E. J. Heller, Phys. Rev. Lett. **104**, 093901 (2010).
[18] M. Shats, H. Punzmann, and H. Xia, Phys. Rev. Lett. **104**, 104503 (2010).
[19] S. Vergeles and S. K. Turitsyn, Phys. Rev. E **83**, 061801(R) (2011).
[20] F. T. Arecchi, U. Bortolozzo, A. Montina, and S. Residori, Phys. Rev. Lett. **106**, 153901 (2011).
[21] A. Chabchoub, N. P. Hoffmann, and N. Akhmediev, Phys. Rev. Lett. **106**, 204502 (2011); J. Geophys. Res. **117**, C00J02 (2012).
[22] B. Kibler, J. Fatome, C. Finot, G. Millot, F. Dias, G. Genty, N. Akhmediev, and J. M. Dudley, Nat. Phys. **6**, 790 (2010).
[23] N. Akhmediev, A. Ankiewicz, and M. Taki, Phys. Lett. A **373**, 675 (2009).
[24] A. Ankiewicz, J. M. Soto-Crespo, and N. Akhmediev, Phys. Rev. E **81**, 046602 (2010).
[25] J. M. Soto-Crespo, Ph. Grelu, and N. Akhmediev, Phys. Rev. E **84**, 016604 (2011).
[26] A. Ankiewicz, N. Akhmediev, and J. M. Soto-Crespo, Phys. Rev. E. **82**, 026602 (2010).
[27] U. Bandelow and N. Akhmediev, Phys. Rev. E **86**, 026606 (2012).
[28] P. Dubard and V. B. Matveev, Nat. Hazards Earth Syst. Sci. **11**, 667 (2011).
[29] Y. Ohta and J. K. Yang, Proc. R. Soc. London, Ser. A **468**, 1716 (2012); Phys. Rev. E **86**, 036604 (2012).
[30] S. W. Xu, J. S. He, and L. H. Wang, J. Phys. A **44**, 305203 (2011); Y. Y. Wang, J. S. He, and Y. S. Li, Commun. Theor. Phys. **56**, 995 (2011); Y. S. Tao and J. S. He, Phys. Rev. E **85**, 026601 (2012); S. W. Xu and J. S. He, J. Math. Phys. **53**, 063507 (2012); J. S. He, S. W. Xu, and K. Porsezian, J. Phys. Soc. Jpn. **81**, 124007 (2012); **81**, 033002 (2012); S. W. Xu, J. S. He, and L. H. Wang, Europhys. Lett. **97**, 30007 (2012); J. S. He, S. W. Xu, and K. Porsezian, Phys. Rev. E **86**, 066603 (2012); C. Z. Li, J. S. He, and K. Porsezian, *ibid.* **87**, 012913 (2013); L. H. Wang, K. Porsezian, and J. S. He, *ibid.* **87**, 053202 (2013); S. W. Xu, K. Porsezian, J. S. He, and Y. Cheng, *ibid.* **88**, 062925 (2013).
[31] G. Y. Yang, L. Li, and S. T. Jia, Phys. Rev. E **85**, 046608 (2012).
[32] B. L. Guo and L. M. Lin, Chin. Phys. Lett. **28**, 110202 (2011).
[33] F. Baronio, A. Degasperis, M. Conforti, and S. Wabnitz, Phys. Rev. Lett. **109**, 044102 (2012).
[34] Z. Qin and G. Mu, Phys. Rev. E **86**, 036601 (2012).
[35] L. C. Zhao and J. Liu, Phys. Rev. E **87**, 013201 (2013).
[36] M. Taki, A. Mussot, A. Kudlinski, E. Louvergneaux, M. Kolobov, and M. Douay, Phys. Lett. A **374**, 691 (2010).
[37] S. H. Chen and L. Y. Song, Phys. Rev. E **87**, 032910 (2013).
[38] Q. L. Zha, Phys. Scr. **87**, 065401 (2013).
[39] L. J. Li, Z. W. Wu, L. H. Wang, and J. S. He, Ann. Phys. **334**, 198 (2013).
[40] J. S. He, H. R. Zhang, L. H. Wang, K. Porsezian, and A. S. Fokas, Phys. Rev. E **87**, 052914 (2013).
[41] M. J. Ablowitz and P. A. Clarkson, *Solitons, Nonlinear Evolution Equations and Inverse Scattering* (Cambridge University Press, New York, 1991).
[42] H. Leblond, H. Triki, F. Sanchez, and D. Mihalache, Opt. Commun. **285**, 356 (2012).
[43] H. Leblond and D. Mihalache, Rom. Rep. Phys. (Suppl.) **63**, 1254 (2011).
[44] G. Neugebauer and R. Meinel, Phys. Lett. A **100**, 467 (1984).
[45] Y. S. Li, X. S. Gu, and M. R. Zou, Acta Math. Sin., New Ser. **3**, 143 (1987).
[46] V. B. Matveev and M. A. Salle, *Darboux Transformations and Solitons* (Springer, Berlin, 1991).
[47] C. H. Gu and Z. X. Zhou, Lett. Math. Phys. **13**, 179 (1987).
[48] C. H. Gu, H. S. Hu, and Z. X. Zhou, *Darboux Trasformations in Integrable Systems* (Springer, Dortrecht, 2006).
[49] J. S. He, L. Zhang, Y. Cheng, and Y. S. Li, Sci. China, Ser. A: Math. **49**, 1867 (2006).
[50] D. J. Kedziora, A. Ankiewicz, and N. Akhmediev, Phys. Rev. E **84**, 056611 (2011).